DEVELOPMENT AND EXPERIMENTAL EVALUATION OF A STATE DEPENDENT COEFFICIENT BASED STATE ESTIMATOR FOR FUNCTIONAL ELECTRICAL STIMULATION-ELICITED TASKS

by

Qiang Zhong

B.S, Zhejiang University, 2014

Submitted to the Graduate Faculty of

Swanson School of Engineering in partial fulfillment

of the requirements for the degree of

Master of Science

University of Pittsburgh

2016

UNIVERSITY OF PITTSBURGH

SWANSON SCHOOL OF ENGINEERING

This thesis was presented

by

Qiang Zhong

It was defended on

April 4, 2016

and approved by

Nitin Sharma, PhD, Assistant Professor

Department of Mechanical Engineering and Materials Science

Zhi-Hong Mao, PhD, Associate Professor

Department of Electrical and Computer Engineering and Department of Bioengineering

William W. Clark, PhD, Professor

Department of Mechanical Engineering and Materials Science

Thesis Advisor: Nitin Sharma, PhD, Assistant Professor

DEVELOPMENT AND EXPERIMENTAL EVALUATION OF A STATE DEPENDENT COEFFICIENT BASED STATE ESTIMATOR FOR FUNCTIONAL ELECTRICAL STIMULATION-ELICITED TASKS

Qiang Zhong, M.S.

University of Pittsburgh, 2016

Functional electrical stimulation (FES) is an application of low-level electrical current to the motor nerves to produce muscle contractions. FES-induced limb motion can be used to reproduce gait in persons with paraplegia. The biggest limitation of using FES for gait restoration is the rapid onset of muscle fatigue. Unlike FES, powered exoskeletons don't suffer from this limitation but need batteries and large actuators to generate enough torque to restore gait motion. However, a hybrid neuroprosthesis that combines these two technologies may be a promising direction to achieve walking for long durations. Our ultimate goal is to develop a wearable hybrid neuroprosthesis that can be conveniently used in daily life.

In order to use closed loop feedback control for a wearable walking hybrid neuroprosthesis, accurate estimates of lower limb angles need to be determined. This thesis presents a nonlinear estimator that parameterizes nonlinearities in an extended linear form using a state-dependent coefficient formulation. The new class of state estimation algorithm is called State-Dependent Riccati Equation (SDRE) based estimator and was implemented on a single joint knee model driven by FES of the quadriceps muscle. Two inertial measurement units (IMUs) were used to measure kinematic data of the thigh and shank segments. To prove that the

SDRE estimator is feasible for this application, it was compared with an Extended Kalman Filter (EKF) and a rotation matrix method (RMX). Each estimator's performance was evaluated using a rotary encoder, which was assumed as the true value of the joint angle. The error for each estimator was calculated through the root mean square error (RMSE), in which the experimental results showed that the SDRE estimator had the most accurate knee joint estimation with a mean RMSE of 1.77°. The EKF and rotation matrix gave a mean RMSE of 2.04° and 2.79°, respectively.

Further, a two limb joint angle simulation study was performed to explore the performance of the SDRE estimator during multi-DOF limb movements. In another simulation, this novel estimator was combined with the synergy-inspired controller scheme for tracking control of hip and knee joint angles. A discussion on stability analysis of this estimator-controller scheme is also presented in this thesis.

TABLE OF CONTENTS

LIST OF TABLES

LIST OF FIGURES

ACKNOWLEDGMENT

First of all, I would have great and sincere thanks to my advisor, Dr. Nitin Sharma for patience, generousness throughout my study and research. Without his guidance and support, I would never accomplish my research.

I would also thank my committee members: Dr. Zhi-Hong Mao, Prof. William W. Clark and Dr. Nitin Sharma for their time to make this thesis better.

I have my thanks to my excellent upper-class students in our lab: Nicholas A. Kirsch and Naji A. Alibeji; thanks for their help in solving technical problems and sharing priceless experience on research. I also thank for Marcus Allen, for his support on Rotation Matrix and IMU. My thanks also go to my lab partners: Xuefeng Bao, Tianyi Qiu for their kind help.

Finally, I would thank my family for their support.

1.0 INTRODUCTION

Every year approximately 5125 people in the USA become paraplegic because of a spinal cord injury (SCI) [1]. That impairs their walking ability and deeply limits activities of daily living. Functional electrical stimulation (FES) is an application of low-level electrical current to the motor nerves to produce muscle contractions that can be used for gait restoration in person with spinal cord injury [2-4]. Walking motion can be achieved by accurately stimulating specific muscle groups in a proper sequence [5]. But the use of FES for gait restoration is limited by the rapid onset of muscle fatigue. Unlike FES, powered exoskeletons don't suffer from this limitation but need batteries and large actuators to generate enough torque to restore gait motion. However, a hybrid neuroprosthesis that combines these two technologies may be a promising direction to achieve walking for long durations. A hybrid neuroprosthesis may preserve the advantages of both FES and powered exoskeletons and avoid their limitations at the same time [6-8]. Moreover, the use of powered exoskeleton in the hybrid system can reduce the unnecessary degree of motion, which can simplify the motion of walking gait and reduce the effort needed for FES [3]. Thus, the hybrid system might be a possible direction to achieve longer walking and preserve the extra benefits of FES such as muscle growth and increase bone density.

Accurate state estimation accuracy and reliable control strategies are two crucial parts for high-performance hybrid neuroprosthesis development. Good tracking performance may not be

achieved without accurate measurement of system states. In our current prototype, encoder embedded inside the electric motor is used to measure system state needed. But further development of hybrid device might require more state variables such as foot reaction forces, arm gestures to detect gait phase or human intent. Use of encoders will be a limitation because its rigid structure is not suitable for a wearable neuroprosthesis. A popular method of measurement uses inertial measurement units (IMUs) that consist of three gyroscopes, accelerometers, and magnetometers, which are small enough to attach to the limbs of a user [9, 10]. Many portable FES systems have been developed with IMUs to measure motion data. However, signal noise and drift always exist in the measurement of IMUs [9, 11-14]. Various filters have been developed to solve this problem, such as the Kalman Filter [9, 15], Extended Kalman Filter (EKF) [16] [17], and complementary filters [18]. These state estimators employ a linear dynamical model or linearized dynamics at every time step to filter signal noise and drift.

In this thesis, a State-Dependent Riccati Equation (SDRE)-based estimator is designed to estimate the joint angle of hip and knee joints during FES-elicited tasks or when a hybrid neuroprosthesis is used. First, an experiment was conducted on a single limb-joint, driven by electrical stimulation of the quadriceps muscle, to evaluate the performance of the SDRE-based estimator. The results of SDRE based estimator were compared with two conventional IMU estimation techniques, namely, RMX and EKF estimation algorithms. The rotation matrix method that related the orientation of the two IMUs in a shared frame of reference to obtain the joint estimation was computed. Then, an EKF method, based on a Jacobian of the musculoskeletal dynamics, was used to compare the estimated the limb joint angles.

Secondly, a simulation study was performed to further explore the performance of this new estimator to estimate 2 limbs joint angles of a fixed hip model. After design and test of the

SDRE based estimator for the fixed hip model, it was coupled with a lower dimensional adaptive controller for a 2-DOF fixed hip model. The controller, which is based on our previous work [19] is inspired by the synergy principle for solving the actuator redundancy problem in the hybrid neuroprosthesis.

Contribution: There are three main contributions of this thesis. The main contribution of this thesis is the design and evaluation of the SDRE estimator for accurate estimation of knee joint movement during FES of the quadriceps muscle. Further contribution is that a two limb joint angle simulation study was performed to explore the performance of the SDC estimator during multi-DOF limb movements. Finally, this novel estimator was combined with the synergy-inspired controller scheme for tracking control of hip and knee joint angles. A discussion on stability analysis of this estimator-controller scheme is also presented in this thesis.

This thesis is organized into chapters as follows: Brief introduction on IMU based motion estimation in Chapter 1. Chapter 2 presents the background information on FES and IMU. A literature review about current estimation algorithm (Kalman filter, extended Kalman filter, complementary filter) is included. Chapter 3 shows the detail of the IMU sensor and test of its performance and signal processing. Estimation algorithm development and the experiment for its evaluation is given in Chapter 4. Chapter 5 demonstrates results from the simulation of estimation algorithm on a 2-DOF fixed hip model and the tracking results of the estimator-controller scheme on the 2-DOF fixed hip model. Chapter 6 briefly discusses the overall conclusion and future work. Appendix A shows Simulink block of estimator-controller scheme. Appendix B presents a framework about stability analysis of estimator-controller scheme.

2.0 BACKGROUND INFORMATION AND LITERATURE REVIEW

Functional electrical stimulation (FES) is a technique that applies low-level current to motor nerves to produce muscle contraction. FES is primarily used to restore function in people with disabilities due to spinal cord injury (SCI) [20]. Sometimes it also referred to as neuromuscular electrical stimulation (NMES). The background information will mainly focus on restoration of lower extremity function by using FES. The earliest use of FES on lower limb was to prevent the foot from dragging during the swing phase [21]. Till now, the application of FES on lower limb can be divided into three directions: prevention of foot drop, restoration of standing and recovery of walking ability [22]. In walking restoration area, pioneering research has been done by [23] that introduced the technique of eliciting a flexion reflex of the knee, hip and ankle by stimulating the peroneal nerve, which can be substituted for the swing phase of walking. The Parastep^{TM} company uses 4-6 surface stimulation of the quadriceps, peroneal nerves to enable a person with paraplegia to walk with a walker [24]. Different from surface stimulation referred above, direct activation and control each muscles by implantable systems is another option to achieve walking restoration. The researchers at Cleveland VA Medical Center used up to 48 muscles under a programmable external stimulator to help subjects to walk with a rolling walker, and some of them even were able to climb stairs [25]. In order to control FES system to perform desired motion, feedback signal is needed for controller to adjust the input of FES system in real-time. The closed-loop control of the FES system relies on sensory information of limbs angles

and angular velocities. Measurement of limb kinematics provides necessary information for a controller to stimulate muscles at the proper time to produce walking motion. The following section discusses estimation techniques for limb kinematics.

2.1 CURRENT MOTION ESTIMATION METHOD

An rotary encoder is a traditional method to measure angle position. The rigid structure of encoder becomes a limitation for application to the human body or soft exo-suit. Optical motion analysis systems (e.g.VICON) use a series of high-speed camera to detect the movement of makers on human body then combine the data to reconstruct motion. The advantage of this method is its accuracy. But such system cannot be applied during field studies because we need to reinstall a series of equipment and recalibrate all of them before operating the system correctly. Another practical method of measurement uses IMUs consisting of gyroscopes and accelerometers. Its small size and ability to provide different type of measurements are advantages of this sensor. But drift and noise always exist in IMU measurements, which are the primary limitations of this sensor. The following section reviews research on three most commonly used estimation methods.

2.1.1 Kalman Filter

A Kalman filter that fuses triaxial accelerometer measurements and triaxial gyroscope signals for ambulatory estimation of human motion was discussed in [15]. Because of the heading drift, this proposed Kalman filter is only suitable for long-term measurement. A Kalman filter for the

estimation of the lower trunk orientation during walking using the measurement of accelerometer and gyroscope was designed in [26]. Besides, they tried to determine the importance of choosing suitable parameters of Kalman filter for different walking speeds by doing a sensitivity analysis. According to their result, the use of the approximated parameters resulted in an improvement in the estimation of about 2° compared to conventional integration result. But the residual errors, were still unsatisfactory, with an RMSE of about 5°. With the optimal configuration of the parameters of the filter, the RMSE was significantly reduced to 0.6°, which shows the importance of choosing the suitable parameters. A flex sensor was used with gyroscope together by [27] to estimate the knee joint angle of an SCI patient, the estimation error is near 6°.

2.1.2 Extended Kalman Filter

Besides the Kalman filter, the extended Kalman filter is another popular technique to deal with the measurement drift of IMU. An extended Kalman filter (EKF) was designed based on the similarities between the kinematics of a two-link robot arm and the kinematics of the human leg in [16]. Their work used the measurement from gyroscope attached on the hip to inform a kinematic model based EKF to estimate the linear distance traveled by a subject. For the displacement over a distance of 3.55 meters, the proposed EKF shows a good estimation performance of total distance with an average error of 6.89 cm compared to the previous experiment with an error of 19.8 cm. Because their works were focused on walking position estimation, this estimation algorithm did not perform well in joint angle estimation, the estimated result of knee joint appeared near 20° error in each trajectory peak. Similar to [16], two different models including lower body kinematic model and switching based model were introduced to

EKF to estimate the joint angles from IMU sensor measurements in [17]. They found that the switching based model performed better on the stance leg, and the other model slightly outperforms in estimating the swing leg motion. This difference shows the importance of choosing a proper dynamic model for estimator construction.

2.1.3 Complementary Filter

Some researchers focused on applying a complementary filter to solve the IMU drift problem. A foot-mounted complementary filter (CF)-aided IMU approach for position tracking in indoor environments was proposed in [18]. This CF is greatly simplified to pre-process the sensor data from IMU sensor and avoid the intermediate step of gyro bias estimation and correction, which greatly decrease the computing time. A reliable gait detection method also was applied to an algorithm that only require input from foot-mounted accelerometer sensors without adding a threshold on gyroscope measurements. This work performed well for position estimation, but its performance for angle estimation need be tested. A wide range comparison between different external sensors for gait estimation was performed by [28]. A complementary filter was designed to combine the measurement of accelerometer and gyroscope, the result of estimation showed it performed better compared to accelerometers alone. The result of this work illustrates the advantage of combing accelerometers and gyroscopes; i.e., the measurement of accelerometer could correct the drift in gyroscope to get better estimation performance.

2.2 INERTIAL MEASUREMENT UNIT

An inertial measurement unit (IMU) is a wearable device that measures a body's angular velocity, linear acceleration and magnetic field surrounding the body. IMU are usually applied to aircraft, including unmanned aerial vehicles (UAVs), spacecraft including satellites and landers [29].

2.2.1 Construction and Operational principles

The IMU usually is a small box containing three accelerometers and three gyroscopes and optionally three magnetometers. The gyroscopes measure how the body is rotating in space. Gyroscopes that placed on each axis will provide angular velocity around each axis. Three accelerometers placed on each axis and measure accelerations on each axis [30]. IMU with magnetometers allows measurement of magnetic field amplitudes mostly to assist calibration against orientation drift.

Figure 1. IMU motion tracking system on the human body. The left figure shows Xsens Xbus Kit, and the right figure shows YOST 3 space sensor system.

2.2.2 Disadvantages

The most obvious disadvantage of using IMUs for motion estimation is that they typically have accumulated error. The conventional method to estimate the angle position continually adds detected changes to its previously-calculated positions. Any errors in measurement, although small, are accumulated from point to point. This process leads to 'drift', or an ever-increasing difference between where the estimated system states, and the real position [31].

Due to integration, a constant error in acceleration measurement can cause a linear error in velocity estimation and a quadratic error in the estimated position that increase with time. A constant error in the angular velocity measurement leads to a constant error in the velocity estimation and a linear error in the angular position estimation; and both errors increase with time.

3.0 IMU SENSOR TEST AND SIGNAL PROCESSING

3.1 IMU TEST

As introduced in Section 2.2, the IMU is a suitable choice for the wearable sensor system development. After comparing IMUs from different manufacturers, the YEI 3-Space made by YOST Inc. was chosen.

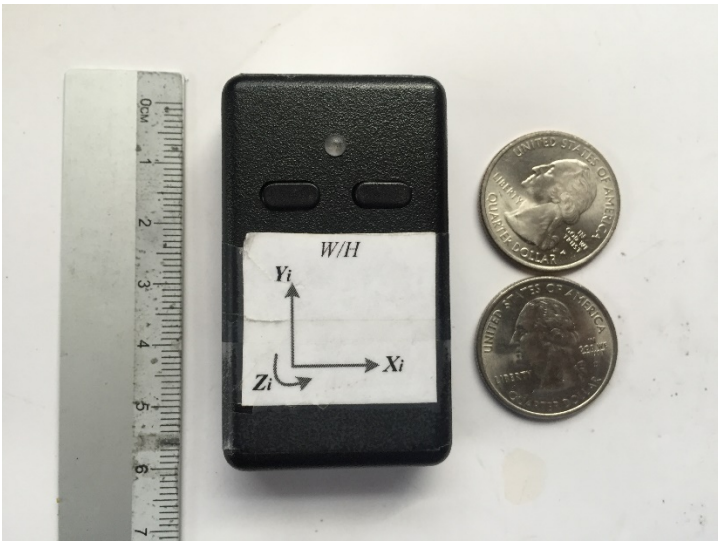

Figure 2. YEI 3-Space IMU sensor

According to the description on its website [32], this sensor is ready-to-use attitude and heading reference system (AHRS) with onboard Kalman filtering algorithm and three

communication interfaces (USB, UART, and SPI). The filtering scheme is shown in Figure 3. This correction algorithm is static calibration that cannot adjust for dynamic environment. The setting of the Kalman filter and its normalization, scale parameters are unknown to the user. Before applying this IMU sensor, a performance test is needed to test its measurement accuracy.

The first test was based on YOST's 3-space sensor suite. It is a software that can provide real-time display of IMU measurement. The motion of IMU sensor is demonstrated by a 3D model. The first step is static position rotation test to evaluate the gyroscope reliability in a static environment. The IMU sensor was put on a horizontal table and rotated in clockwise for one circle and rotated in counter-clockwise for one circle, then repeated it for ten times. As Figure 4 shows from left to right are the different states of IMU during the test. In the static position rotation

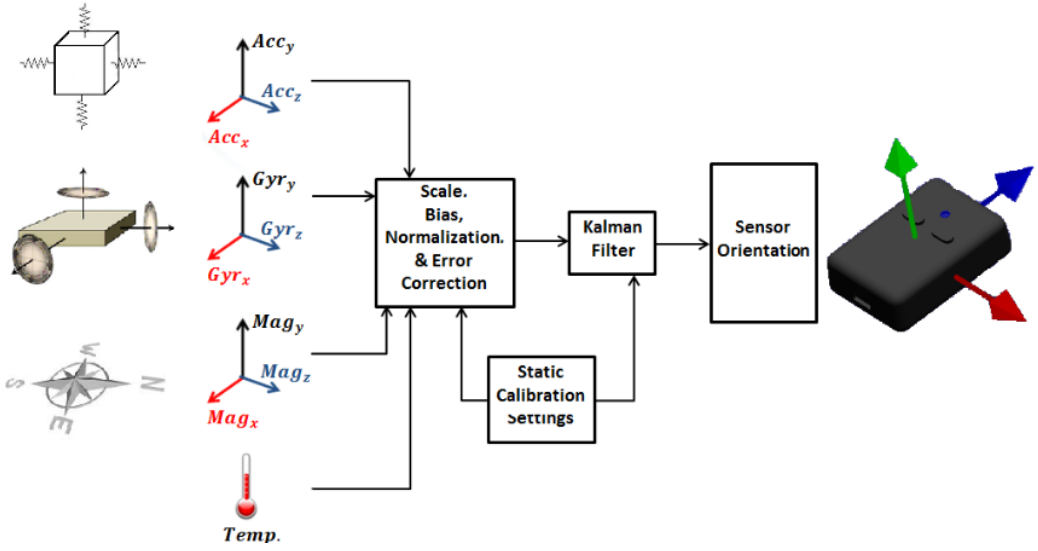

Figure 3. On board filtering scheme with Kalman filter of YEI 3-Space Sensor

test, the IMU performed very well with a slight angle error, as shown in the middle status in Figure 4. But the drift appeared on both X and Y-axis when the IMU moved parallel to another position. As shown in the last status of the IMU in Figure 4, the angle error increased due to the measurement drift of gyroscope. As the result shows, the traditional method, which computes the angle by integrating the measurement of the gyroscope, is not reliable in limb angle estimation.

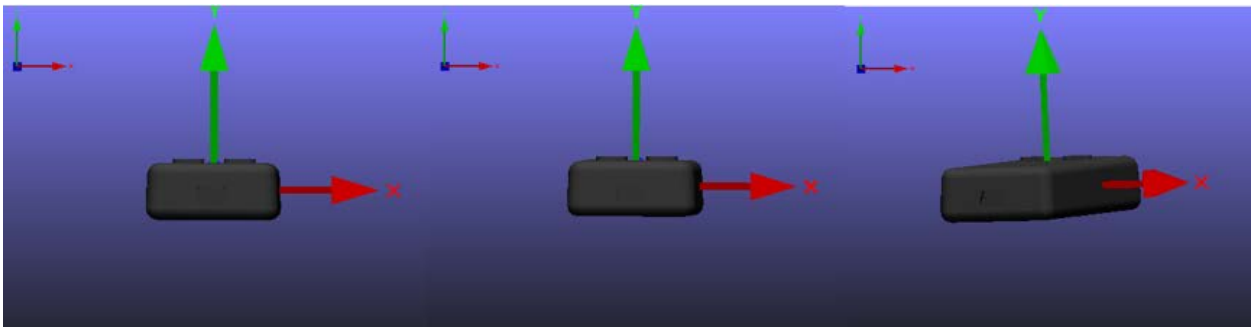

Figure 4. Rotation test of IMU sensor

Therefore, our goal was to use a dynamic model based estimator to correct IMU drift in limb-angle estimation.

3.2 SIGNAL PROCESSING

In order to get pure gravitational acceleration measurement, the motion acceleration must be filtered out. A single differentiation operation, at each data point, must be applied to the gyroscope's measurement to get motion acceleration then subtracted from the measurement of acceleration from the accelerometer. But this differentiation operation aggravates measurement noise in the measurement. Moreover, the measurement from the accelerometer and gyroscope

always contains significant noise, which makes it impossible to apply them directly. A popular method is to apply a low-pass filter to separate noise before the operation. While the walking motion studied in this thesis is slow, the low pass filter will not distort useful information in measurement signals. A 3rd Butterworth filter with a normalized cutoff frequency of 0.05 HZ was designed to get a smooth signal from the raw measurement. Sample signals were collected from one joint limb experiment to guarantee the proposed filter will work in the real situation. As Figure 5 shows, from the beginning to sample point 2500 is a static period, and the dynamic period is from sample point 2500 to 35000, then followed by another static period. The detailed figure shows the filter performed quite well both in the dynamic period and static period. Note there exists a small delay introduced by low pass filter in the dynamic period.

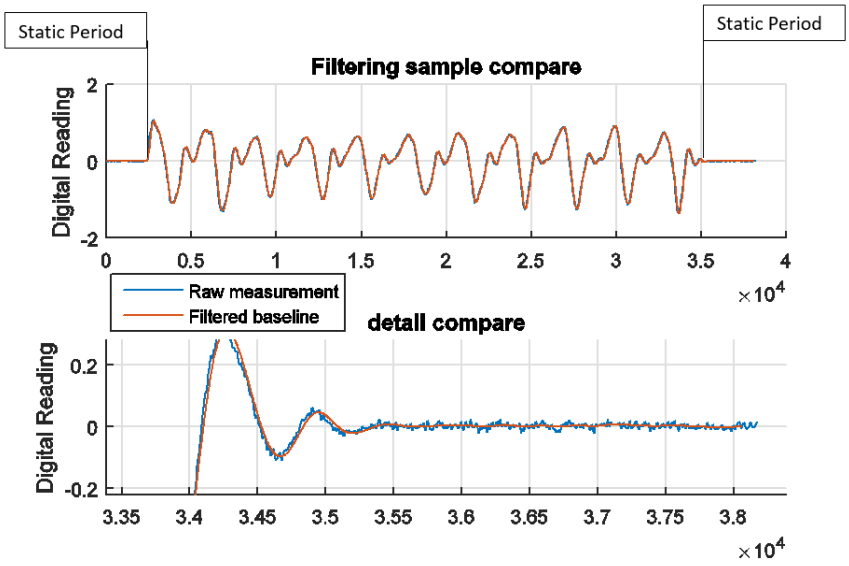

Figure 5. Baseline signal of the angular velocity

Numerical differentiation result of the gyroscope noisy signal after the operation can be superposed on the filtered result to study the influence of low pass filter.

As shown in Figure 6, numerical differentiation operation magnified noises significantly. The angular acceleration signal (Blue) was computed by applying a single differentiation operation on gyroscope signal. Compared to the result of filtered signal (Red), the numerical differentiation greatly magnified over all sample points. For measurements of the accelerometer, the smoothing operation is needed before apply them to the estimator. The 3rd low pass filter was performed on sample signal, the result is shown in Figure 7. The low pass filter dismissed most noise in the peaks of the signal while it is the most valuable part for state estimation that will influence the estimated trajectory peak amplitude.

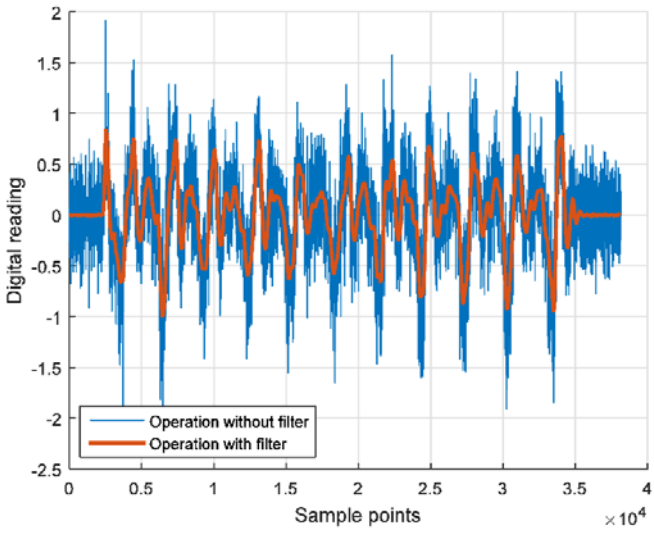

Figure 6. Compare between filtered and nonfiltered numerical differentiation result with sampling time 0.01s.

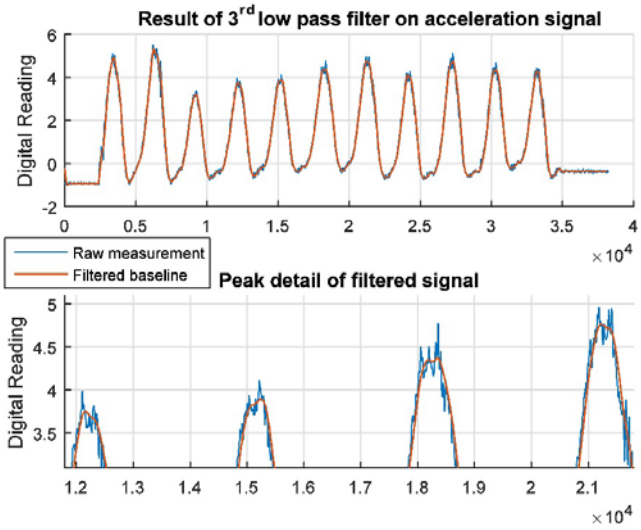

Figure 7. Filter effects on acceleration measurement

As for acceleration measurement, only gravitational acceleration projection on X-axis of IMU is chosen for estimation. But the actual measurement from X-axis is a combination of motion acceleration projection and gravitational acceleration projection, the motion acceleration, however small, needs to be eliminated. The motion acceleration can be approximated by

$$\alpha_{motion} = \ddot{q}L_l, \tag{3.1}$$

where $\ddot{q}$ can obtain from the measurement of the gyroscope after one numerical differentiation operation with sampling time 0.01s, the L_l is the length from IMU position on the limbs to the limb joint. As Figure 8 shows, the amplitude of motion acceleration ranges from -0.2 to 0.25 m/s^2 in the sample signal, which is only about 5% of the amplitude of gravitational acceleration measurement. In this slow motion experiment, the body motion is negligible and can be ignored or use low pass filter to eliminate noise.

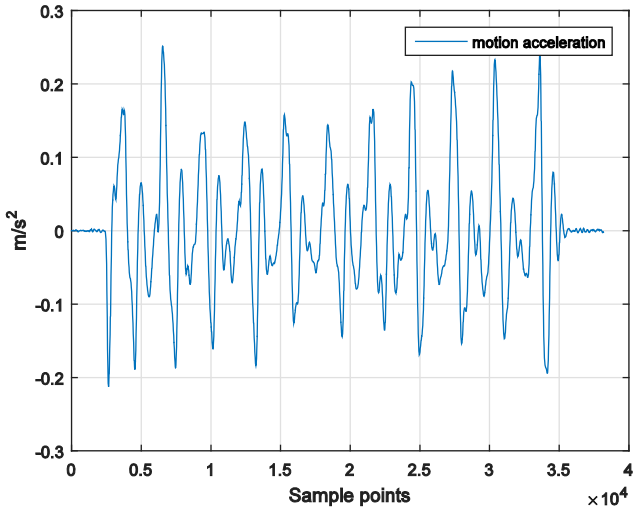

Figure 8. Approximated motion acceleration

Because the amplitude of motion acceleration is negligible, this is the reason why gravitational acceleration projection on X-axis of IMU is chosen in the measurement model for estimator construction. In slow motion case, the motion acceleration is too small to measure accurately, it might be mixed with measurement noise and the useful signal might be eliminated by the low pass filter. The amplitude of gravitational acceleration is much larger than the signal noise that essential signal won't be eliminated by the low pass filter as noise.

3.3 IMU ALIGNMENT

Before the data was processed in the estimator, it must be transformed from the IMU frame to the respective body coordinate systems (CS). This transformation was essential for the estimation process because the system dynamics were modeled in the body CS, especially in the

sagittal plane of the subject. The correlation exists between the know motion vector and IMU measurement vector is:

$$\vec{v}^{\,b} = R_i^b \vec{v}^{\,i}, \tag{3.2}$$

where $\vec{v}^{\,b} \in \mathbb{R}^3$ is the motion vector in the body frame, and $\vec{v}^{\,i} \in \mathbb{R}^3$ is IMU reading vector in the IMU frame and $R_i^b \in \mathbb{R}^{3\times3}$ is the transpose of the alignment matrix that transforms the coordinates from the IMU to the body frame. By defining the body segment frame with axes $(X_b \quad Y_b \quad Z_b)$ and the IMU frame with axes $(x_i \quad y_i \quad z_i)$. The alignment matrix R_b^i can be expressed as follow:

$$R_b^i = \begin{bmatrix} \cos(X_b, x_i) & \cos(Y_b, x_i) & \cos(Z_b, x_i) \\ \cos(X_b, y_i) & \cos(Y_b, y_i) & \cos(Z_b, y_i) \\ \cos(X_b, z_i) & \cos(Y_b, z_i) & \cos(Z_b, z_i) \end{bmatrix} = \begin{bmatrix} X_x & Y_x & Z_x \\ X_y & Y_y & Z_y \\ X_z & Y_z & Z_z \end{bmatrix},$$

where $\cos(X_b, y_i)$ means the cosine of the angle between axis X_b and y_i. When a motion along the axis X_b is performed on IMU, the normalized sensor output vector will be the first column of this matrix. The rest elements can be computed by same method on Y_b and Z_b axis. In order to obtain this alignment matrix, the procedure was performed as shown in Figure 9. The first step is that the subject was asked to stand still for a minimum of 10 seconds. In this time frame, the gravitational acceleration measured by the accelerometer was used to create gravity vector that is coincident with the anatomical axis Z_{th} and Z_{sh} for the two body coordinate systems (CSs, body CS of thigh and shank). Then the subject performed three to five hip extension/flexion rotations. During each positive rotation to let the gyroscopes measure the angular velocity about the horizontal axis X_{th} and X_{sh}. Here we denote the alignment matrix R_{ish}^{bsh} and R_{ith}^{bth} can be written as follow:

$$R_{i*}^{b*} = [\boldsymbol{c}_1 \quad \boldsymbol{c}_2 \quad \boldsymbol{c}_3]$$

where $\boldsymbol{c}_i$ means the columns of the matrix. The acceleration measurement in first step was averaged and normalized to unity to obtain the $\boldsymbol{c}_3$ of the matrix. The readings from gyroscope in second step was integrated and normalized to unity create the $\boldsymbol{c}_1$ of the matrix. Then the $\boldsymbol{c}_2$ was obtained by the product of $\boldsymbol{c}_1$ and $\boldsymbol{c}_3$. Due to the measurement noise and slight difference between motions, transformation result by this initial computed alienation matrix may not accurate.

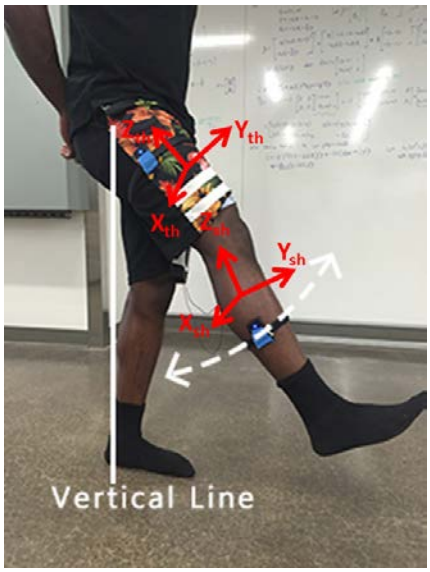

Figure 9. IMU Alignment Procedure

The body axis obtained by this initial alignment matrix may not complete orthogonal to the each other. This was corrected by using pure rotation matrix properties as given below

$$\begin{aligned} \|r_i\| &= \|c_j\| = 1, \\ r_i \bullet r_j &= 0, \\ c_i \bullet c_j &= 0, \end{aligned} \tag{3.3}$$

where $r_i,(i=1,2,3)$ and $c_j,(j=1,2,3)$ represent the designated matrix row and column, respectively. After an orthogonal CS had been created for each body segment, this corrected result may still does not matched the actual body frame, there might existed a deflection around the Z axis. Another correction was needed to rotate the whole CS around the Z-axis to let the Y-axis match the anterior direction. This rotation was constrained to the X-Y plane after the orthogonal correction was made, which simplified the procedure. The angle of rotation was calculated by choosing the first created X-axis as a reference and summing the angles between it and the rest of the X and Y-axis calculated. This was then averaged and subtracted by 45 degrees. This can be seen as follows

$$\theta = \frac{\sum_{i=1}^{n} \theta_{xx} + \theta_{xy}}{2n} - 45^o, \tag{3.4}$$

where θ_{xx} is the angle between the X-axis and the reference X-axis is, θ_{xy} is the angle between the Y-axis and reference X-axis and n is the number of positive rotations. If the Y-axis are perfectly aligned, the θ should be zero. Then this angle was inserted into a correction matrix that rotates the CS around the Z axis as follows

$$\begin{bmatrix} Z_1^2W + c_\theta & Z_1Z_2W - Z_3s_\theta & Z_1Z_3W + Z_2s_\theta \\ Z_1Z_2W + Z_3s_\theta & Z_2^2W + c_\theta & Z_2Z_3W - Z_1s_\theta \\ Z_1Z_3W - Z_2s_\theta & Z_2Z_3W + Z_1s_\theta & Z_3^2W + c_\theta \end{bmatrix}, \tag{3.5}$$
$$W = 1 - c_\theta,$$

where $Z_i,(i=1,2,3)$ is the respective element of the Z-axis vector, $c_\theta = \cos(\theta)$ and $s_\theta = \sin(\theta)$. Then the X axis computed by initial alignment matrix was corrected and final Y-axis can be computed by the cross product of the Z and the new corrected X-axis. The corrected final R_b^i can

be obtained by the operation showed above. Then the IMU data was transformed to the body frame by multiplying each dataset in time by the transpose of the alignment matrix.

4.0 OFFLINE MOTION ESTIMATION

This chapter focused on exploring State-Dependent Riccati Equation (SDRE) based estimator. Simplified models were introduced to do offline estimation experiment and simulation to evaluate the performance of the SDRE estimator, and the results were compared to two conventional IMU estimation techniques. First was the rotation matrix method that related the orientation of the two IMUs in a shared frame of reference to obtain the joint estimation. Followed by a dynamic based Extended Kalman Filter (EKF), which used Jacobian to handle nonlinearities of the system instead of the SDC parameterization. For fixed hip model based two joint simulation, only EKF was compared to SDRE estimator.

4.1 OFFLINE ESTIMATION ON LEG EXTENSION MACHINE

In order to explore the performance of SDRE estimator, a single link dynamic model of the leg in a leg extension machine with stimulation of the quadriceps was chosen.

4.1.1 Single joint Dynamic and Measurement model

The dynamics of a leg extension musculoskeletal system with FES applied in Figure 10 is given by

$$J\ddot{\theta} + G(\theta) = T_P + T_{ke}, \tag{4.1}$$

where $J \in \mathbb{R}$ denotes the moment of inertia lower leg, $\theta, \dot{\theta}, \ddot{\theta} \in \mathbb{R}$ are the angular position, velocity, and acceleration of the lower leg (shank and foot) relative to equilibrium. $G(\theta) = mgl_c \sin(\theta + \theta_{eq})$ is the gravitational torque where m is the mass of lower leg, g is gravitational acceleration, l_c is the length from the mass center of the lower leg to the knee joint and θ_{eq} is the equilibrium angle relative to vertical. T_p represents the passive musculoskeletal torque of the knee joint, which is modeled as

$$T_p = d_1(\phi - \phi_0) + d_2\dot{\phi} + d_3 e^{d_4\phi} - d_5 e^{d_6\phi}, \tag{4.2}$$

where d_i, $(i = 1, 2, ..6)$ and ϕ_0 are subject specific parameters that model the stiffness and damping of the knee joint. In this part, ϕ and $\dot{\phi}$ represents the anatomical knee joint angle and angular velocity, respectively. Each variable can be defined as $\theta + \theta_{eq} = \frac{\pi}{2} - \phi$ and $\dot{\phi} = -\dot{\theta}$.

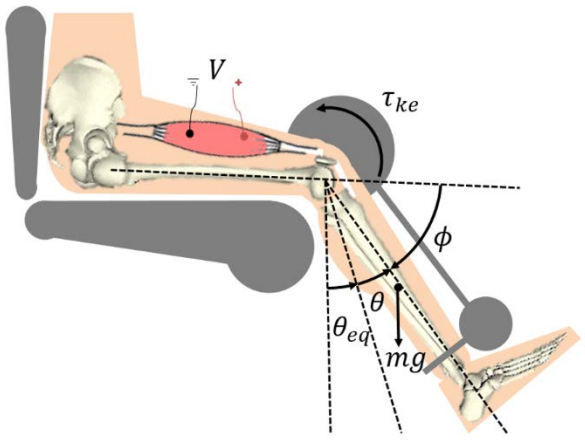

Figure 10. Leg extension musculoskeletal model

From (4.1), T_{ke} is torque produced by muscle contraction caused by FES, it is modeled as:

$$T_{ke} = (\mathrm{c}_2 \phi^2 + \mathrm{c}_1 \phi + \mathrm{c}_0)(1 + \mathrm{c}_3 \dot{\phi}) a_{ke}, \tag{4.3}$$

where C_i, $(i = 0,1,2,3)$ represent the force-length parameters of the dynamic model. The muscle activation a_{ke} parameter dynamic can be ignored and assumed equal to $u_{ke} \in [0,1]$ which the normalized electrical stimulation amplitude. The normalized electrical stimulation amplitude can be mapped to the current amplitude of the electrical stimulation as:

$$I = I_t + u_{ke}(I_s - I_t), \tag{4.4}$$

in which I_t and I_s represent the minimum current amplitude required to produce a movement (threshold) and the minimum current amplitude that produces the maximum muscle force (saturation), respectively. The dynamic model of this system can be expressed as follow:

$$\dot{x} = f(x,u) + w, \tag{4.5}$$

where $w = \begin{bmatrix} 0 & \bar{w} \end{bmatrix}^T \in \mathbb{R}^2$ is a process noise characterized by Gaussian process and an associated covariance matrix $Q \in \mathbb{R}^{2\times 2}$, and the nonlinear function $f(x,u) \in \mathbb{R}^2$ is given by

$$f(x,u) = \begin{bmatrix} x_2 \\ -\beta \sin(x_1) + \alpha(T_p + T_{ke}) \end{bmatrix} \tag{4.6}$$

where $x = \begin{bmatrix} x_1 & x_2 \end{bmatrix}^T = \begin{bmatrix} \theta + \theta_{eq} & \dot{\theta} \end{bmatrix}^T$ with $\alpha = 1/J, \beta = mgl_c\alpha$.

The IMU attached to the shank provided three kinds of measurements: three-axis angular velocities, linear accelerations and magnetic amplitude from the gyroscopes, accelerometers, and magnetometers. During these experiments, the motion of the leg was slow enough (just like the case of FES and orthosis based walking) that we assumed that the accelerometer only measured the gravitational acceleration, the motion acceleration part can be considered as the noise in

acceleration measurement. Thus, the measurements from the IMUs can be expressed as follows, and signal was filtered by a low pass filter before being applied to measurement model

$$y = h(x) + v = \begin{bmatrix} h_1 & h_2 \end{bmatrix}^T + v, \tag{4.7}$$

$$h_1 = x_2,\ h_2 = -g\sin(x_1),$$

where h_1 denotes the measurement from the Z-axis gyroscope of IMU after transformation by alignment matrix, and h_2 denotes the measurement from X-axis accelerometer of IMU after transformation by alignment matrix. The v is a two dimensional zero-mean Gaussian measurement noise with the measurement covariance matrix $S \in \mathbb{R}^{2\times 2}$.

4.1.2 State-Dependent Coefficient (SDC) Parameterization

The SDRE estimator is based on the dynamic model presented in (4.5) and measurement model (4.7). Unlike the EKF, which uses a Jacobian to approximate the dynamics of the system, the SDRE estimator implements the SDC form approximation. The advantage of the SDC based approximation is that it is not unique and yields multiple estimators, with each of them has different performance, and SDC parameterization process won't cause mismatch compare to the original system. It was assumed that the nonlinear dynamics can be directly inserted into state-dependent form by SDC parametrizations as shown below:

$$\begin{aligned} \dot{x} &= A_i(x)x + B(x)u + w \quad \forall i = \{1..n\}, \\ y &= C_j(x)x + v \qquad \forall j = \{1..\mathrm{m}\}, \end{aligned} \tag{4.8}$$

$A_i(x)$ and $C_j(x)$ are nonlinear matrices, both of them satisfy following conditions:

$$A(\gamma_i, x, t)x = \gamma_1 A_1(x,t)x + \gamma_2 A_2(x,t)x + \ldots + \gamma_n A_n(x,t)x, \tag{4.9}$$

where $\gamma_i \geq 0$ and $\sum_{i=1}^{n} \gamma_i = 1$.

$$C(\delta_j, x, t)x = \delta_1 \mathrm{C}_1(x,t)x + \delta_2 \mathrm{C}_2(x,t)x + ... + \delta_m \mathrm{C}_m(x,t)x, \tag{4.10}$$

where $\delta_j \geq 0$ and $\sum_{j=1}^{n} \delta_j = 1$.

There exist clear requirements for choosing suitable SDC parameterization form.

Remark1: The SDC parameterization matrix $A_i(x)$ and $C_j(x)$ should not go to infinity for any x during the estimation process.

Remark2: The SDC parameterization matrix $A_i(x)$ and $C_j(x)$ should be of both full ranks.

By defining $\sin c(x) = \frac{\sin(x)}{x}$, and because $\lim_{x \to 0} \sin c(x) = 1$, a suitable SDC parameterization of (4.5) was chosen as follows:

$$A(\hat{x}) = \begin{bmatrix} 0 & 1 \\ -\beta \sin c(\hat{x}_1) & 0 \end{bmatrix}, \tag{4.11}$$

$$B(\hat{x})u = \begin{bmatrix} 0 \\ \alpha(T_p + T_{ke}) \end{bmatrix}, \tag{4.12}$$

$$C(\hat{x}) = \begin{bmatrix} 0 & 1 \\ -g \sin c(\hat{x}_1) & 0 \end{bmatrix}. \tag{4.13}$$

The SDRE estimator is given by

$$\dot{\hat{x}} = A(\hat{x}, t)\hat{x} + B(\hat{x}, t)u + K(\hat{x}, t)(y - C(\hat{x}, t)\hat{x}), \tag{4.14}$$

the $K \in \mathbb{R}^{2\times 2}$ is obtain from

$$K(\hat{x}, t) = P(\hat{x}, t)C^T(\hat{x}, t)S^{-1}, \tag{4.15}$$

the $S \in \mathbb{R}^{2\times 2}$ is the measurement noise covariance matrix and the $P(\hat{x}, t) \in R^{2x2}$ is a positive symmetric solution to

$$\begin{aligned}\dot{P}(\hat{x},t) = \quad & A(\hat{x},t)P(\hat{x},t) + P(\hat{x},t)A^T(\hat{x},t) + 2aP(\hat{x},t) \\ & -P(\hat{x},t)(C^T(\hat{x},t)S^{-1}C^T(\hat{x},t))P(\hat{x},t) + Q,\end{aligned} \tag{4.16}$$

The estimator gain $a = 1$ was chosen in this case.

The zero-mean Gaussian noise process with the covariance matrices $Q \in \mathbb{R}^{2\times 2}$ and $S \in \mathbb{R}^{2\times 2}$ are given by

$$\begin{aligned} Q &= \begin{bmatrix} n_1 & 0 \\ 0 & n_2 \end{bmatrix}, \\ S &= \begin{bmatrix} s_1 & 0 \\ 0 & s_2 \end{bmatrix}. \end{aligned} \tag{4.17}$$

The process noise matrix Q is a constant diagonal matrix, where the n_1, n_2 terms were determined by tuning for the best performance based on one trial that was performed before the experiment. S represents the constant measurement noise matrix that was calculated by taking the sample standard deviation of the filtered IMUs measurement data in the initialization stage when the IMUs were stationary.

4.1.3 Experiment implementation

The experimental setup is shown in Figure 11 where the rotary joint of the leg extension machine can be fixed at different angles so that the force can be measured by the load cell. Three able-bodied persons participated in the experiment, where each leg was identified as a separate subject.

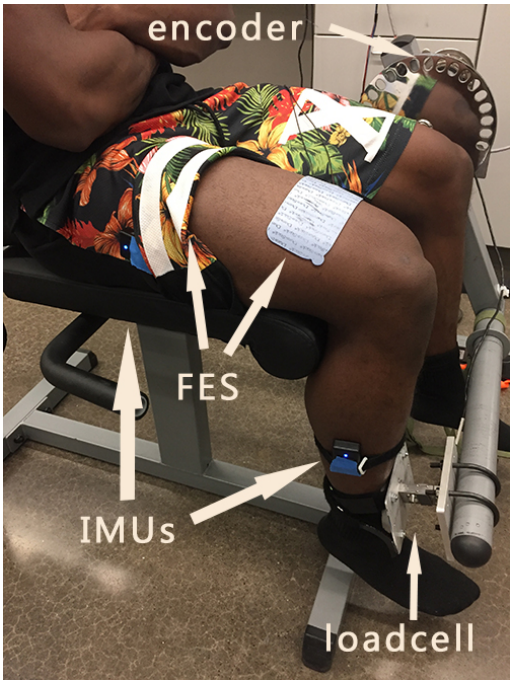

Figure 11 Subject sitting in the leg extension machine

The parameters of dynamics of each subject were determined by a system identification process as described in [33]. All results of parameter estimation are shown in Table 1.

Table 1. Subject parameters obtained from the parameter estimation procedure. L and R represent the subject's left and right leg respect

$\phi_0 [rads]$	0.40	8.34E-11	0.78	2.22E-14	0.30	1.50
$d_1 [Nm]$	4.05	2.27	5.86	4.12	2.22E-14	4.41
$d_2 [Nm]$	3.05	3.30	3.56	2.54	3.14	2.60
$d_3 [Nm]$	1.48E-9	3.96E-8	1.54E-5	2.38E-5	6.1984	3.39E-4

Table 1 (continued)

d_4	14.10	11.20	8.70	8.33	0.84	6.70
$d_5\left[Nm\right]$	8.90	15.30	3.05	5.41	0.04	0.16
d_6	-1.76	-1.77	-3.45	-0.41	-30.22	-1.26E-8
$c_0\left[Nm\right]$	76.71	61.00	27.74	-28.29	-17.88	5.63
$c_1\left[Nm\right]$	3.12	-0.57	296.32	402.07	299.41	159.39
$c_2\left[Nm\right]$	-15.36	-8.47	-186.11	-231.19	-183.75	-85.94
c_3	0.28	0.47	1.93E-4	0.88	1.52	1.75
$\theta_{eq}\left[rads\right]$	0.13	0.08	0.19	0.17	0.17	0.14
$T_a\left[Sec\right]$	0.25	0.19	0.14	1.0	0.72	0.18
$I_t\left[mA\right]$	33.90	38.60	33.50	38.80	38.20	32.90
$I_s\left[mA\right]$	60.40	68.20	66.60	64.90	68.10	63.20
$RMSE\left[Deg\right]$	2.61	3.42	2.43	4.06	4.18	3.15

As Figure 11 shows, two IMUs were placed firmly on the thigh and shank segments of the leg using an electrical tape. The wireless communication between the IMUs and the wireless dongle was established in a program written in Matlab 2015a with a sampling frequency of 100Hz. The encoder data was acquired in a Matlab Simulink file with a higher sample frequency of 1000Hz. Because the sampling rates between the two pieces of equipment did not match, the IMU data was interpolated by using Matlab' s cubic spline data interpolation function and then

filtered by a 3rd low pass filter. The experimental testing done on leg extension machine was conducted on three healthy persons. Each subject performed three tests per leg, which created a total of 18 trials. To assess the performance of the system, the subject's motion was recorded using a rotary encoder (type: GHH100, by CALT, China) in leg extension machine. The results produced from SDRE estimator and IMUs are shown for one of the experiments and compared against the estimated results from the EKF, RMX method and the data collected from the encoder.

4.1.4 Result and discussion of single joint experiment

We noticed that during the offline estimation, some parameters of the model had changed. Especially the threshold value and the initial angle of the dynamic model, and these parameters could affect the overall estimation value. In order to fix this problem, the threshold value was adjusted to a value that used in experiment instead of the original one we got from the system identification (Note: A pre-trial test by setting different level threshold around the value we got from system identification was performed on each subject to determine a suitable threshold value for experiment). For the initial angle, the acceleration signal measured at the beginning of the experiment, when subject’s shank was stationary was used to calculate the initial angle. After these two operations, the estimation result of both SDRE estimator and EKF showed good tracking performance.

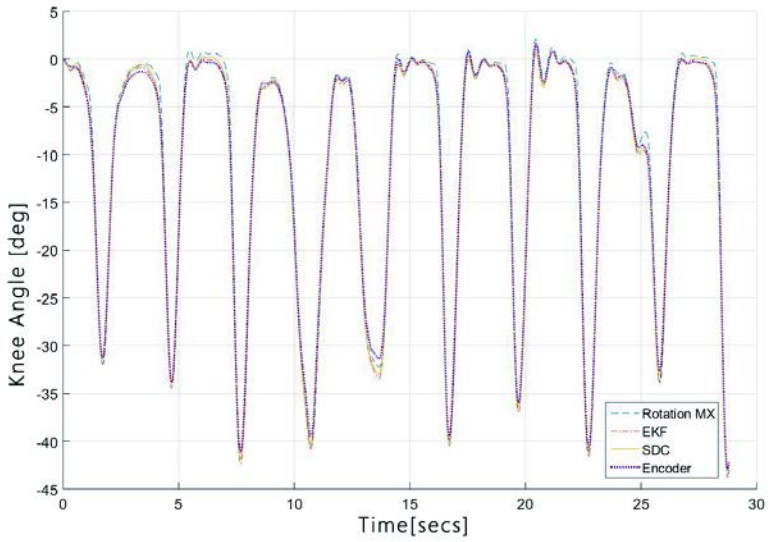

Figure 12. Full view of the knee joint angle estimation during the single joint experiment

Three 30 second long experiments were performed on each subject, and all these three estimators performed offline estimation on each trail. Figure 12 is a representative comparison between each estimator for subject 2 (trial 2). The results show that each estimator displays the overall characteristics of the knee joint angle as it transitions from knee flexion to extension, but the majority of the error occurred at the upper and lower peaks of the curves. The SDRE estimator and EKF compensated for most of the drifts in IMUs during upper and lower peaks as compared to the RMX method. The SDRE estimator and EKF only used the measurement from IMU on shank and RMX used the measurement from both IMU sensors. Results of 3 trials (trail 2 and 3 of P1-R and trial 3 of P3-R) of RMX were unavailable because the IMU on thigh drop some data during the experiment. Table 2 shows all root mean square error (RMSE) of the estimation results of these three methods. A Shapiro-Wilk test was used to determine if the RMSE data were normal data sets.

Table 2. Comparison RMSEs of the SDRE-Estimator (SDC), Extended Kalman Filter (EKF) and Rotation Matrix (RMX)

	P1-L			P1-R			P2-L			
Trial	1	2	3	1	2	3	1	2	3	
SDC	1.10	1.77	1.19	1.78	1.64	1.55	1.25	0.77	1.05	
EKF	1.28	3.00	1.06	1.90	1.62	1.67	1.29	0.92	1.07	
RMX	3.39	3.22	2.55	1.95	NA	NA	2.39	0.94	0.99	
	P2-R			P3-L			P3-R			
Trial	1	2	3	1	2	3	1	2	3	Avg RMSE
SDC	2.01	2.07	2.10	2.01	2.79	2.0	2.45	2.49	2.40	1.77
EKF	2.11	2.80	2.57	2.20	2.86	1.73	2.95	2.86	2.82	2.04
RMX	3.53	6.06	5.92	2.95	2.06	2.49	2.20	1.26	NA	2.79

- Note: the unit of RMSE is degree

From the results of the Shapiro-Wilk test, it was showed that the RMSE data sets are not normal distributions. Therefore, a Wilcoxon signed rank test with a 95% confidence level was used to determine if there was a difference between these estimators. As shown in Figure 14, the test result between SDRE and EKF shows the significant index is 0.005 which means there exist a significant difference between the result of SDRE estimator and EKF. Similar, the test result between SDRE and Rotation Matrix is 0.035 that there exist a significant difference between the result of SDRE and Rotation Matrix. Therefore, it can be concluded that SDRE estimator improved the estimation performance compare to these two methods in this case.

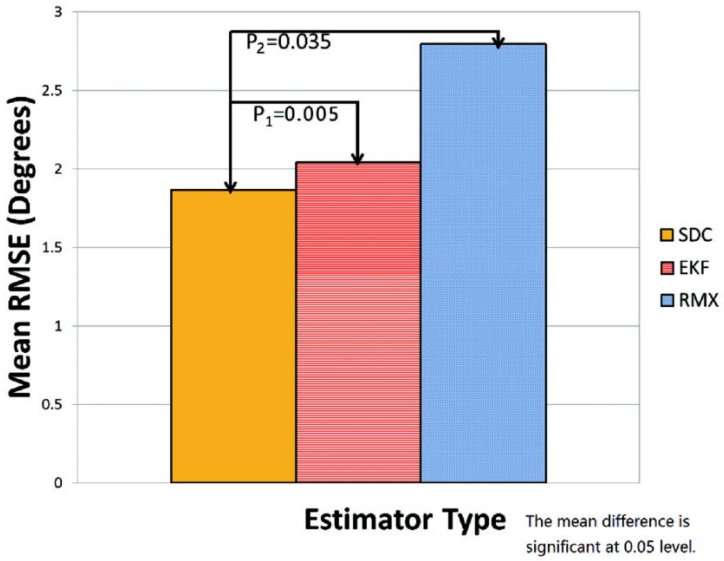

Figure 13. Result of Wilcoxon-signed rank test

In the experiment, as expected, both SDRE estimator and EKF enhanced the estimation of the knee joint angle by reducing the error between the true and estimated peaks. It is because both SDRE estimator and EKF are dynamic based, they can correct the measurement drift by model predict value. Compared the SDRE performance to EKF's and Rotation Matrix's, the SDRE estimation result was better based on the statistical analysis result. For SDRE estimator, the major error occurred at peaks in the experiment. The most obvious reason is that error could result from the parameter estimation. As shown in Table 1, the RMSE of parameter identification usually around 2° to 4°, which indicates the estimation error may be mainly caused by inaccurate dynamic parameters. And we estimated the parameters before the experiment, the subject characteristics may have changed when the experiments were performed. Especially threshold value of dynamic model may deeply influence the peak value. Another assumption is that error in defining the body frame may have caused the estimators to predict the next position incorrectly which could propagate throughout the experiment. With this error, the orientation of

the sagittal plane can be slightly offset, in which the dynamic model doesn't properly compensate for this situation.

In order to explore the difference of SDRE-estimator and EKF for the more complex nonlinear system, a 2 DOF fixed hip model was used to do a simulation study.

4.2 OFFLINE ESTIMATION ON 2-DOF FIXED HIP MODEL

4.2.1 Fixed hip dynamic model and measurement model

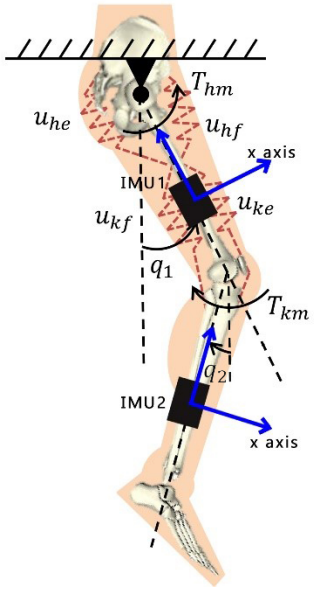

Figure 14. A schematic of the fixed hip model with no ground model. The $u_{he}, u_{hf}, u_{ke}, u_{kf}$ indicate the input to the stimulated muscles which produce hip/knee flexion and extension and the torques produced by the motors at are labeled as T_{hm}, T_{km}.

The dynamics equation of a fix hip hybrid neuroprosthesis with 2-DOF shown in Figure 14 is given by:

$$M(q)\ddot{q} + V(q,\dot{q}) + G(q) = T_{Pa} + T\,, \tag{4.18}$$

where $M(q) \in \mathbb{R}^{2\times 2}$ denotes the combined moment of inertia of the orthosis and human limbs, $V(q,\dot{q}) \in \mathbb{R}^2$ is the Coriolis vector, $G(q) \in \mathbb{R}^{2\times 2}$ is the gravitational torque vector, $q, \dot{q}, \ddot{q} \in \mathbb{R}^2$ are the angular position, velocity, and acceleration of the segments of the swinging leg relative to equilibrium. $T_{Pa} \in \mathbb{R}^2$ represent the passive musculoskeletal torque vector of the knee joint and hip joint. Activate torques at joints are produced by musculoskeletal dynamics due to FES and electric motor, it is defined as follow:

$$T = b(q,\dot{q})u\,, \tag{4.19}$$

where $u(t) \in \mathbb{R}^6$ and $b \in \in \mathbb{R}^{2\times 6}$ is the control gain matrix as follow:

$$b = \begin{bmatrix} \psi_{h_{fx}} & 0 \\ 0 & -\psi_{h_{ex}} \\ \psi_{k_{fx}} & 0 \\ 0 & -\psi_{k_{ex}} \\ \kappa_h & 0 \\ 0 & \kappa_k \end{bmatrix}^T . \tag{4.20}$$

$\psi_{h_{fx}}, \psi_{h_{ex}}, \psi_{k_{fx}}, \psi_{k_{ex}}$ are torque length and torque-velocity relationships of the flexor and extensor muscles at hip and knee joints, respectively, κ_1, κ_2 are the conversion gain of the electric motor to converge current to torque.

4.2.2 Fix hip SDC parameterization

Define the state vector as follows:

$$\begin{aligned} x &= [x_1, x_2, x_3, x_4]^T, \\ x_3 &= \dot{x}_1, x_4 = \dot{x}_2. \end{aligned} \tag{4.21}$$

In order to meet requirements of state dependent coefficient parameterization, defining the clockwise direction as negative, set $x_1 = q_1$, $x_2 = q_2$, such that the dynamic of the hybrid device can be expressed as follow:

$$\dot{x} = f(x,u) + w, \tag{4.22}$$

where $w = \begin{bmatrix} 0 & 0 & \overline{w}_1 & \overline{w}_2 \end{bmatrix}^T \in \mathbb{R}^4$ is a process noise characterized by Gaussian process and an associated covariance matrix $Q \in \mathbb{R}^{4\times4}$, and the nonlinear function $f(x,u) \in \mathbb{R}^4$ is given by

$$f(x,u) = \begin{bmatrix} x_3 \\ x_4 \\ M^{-1}(x)(-V(x) - G(x) + T_{pa} + T) \end{bmatrix} \tag{4.23}$$

where

$$M^{-1}(x) \triangleq \begin{bmatrix} w_{11} & w_{12} \\ w_{21} & w_{22} \end{bmatrix},$$

$$V(x) = \begin{bmatrix} a_1 x_4^2 \sin(x_1 - x_2) \\ -a_1 x_3^2 \sin(x_1 - x_2) \end{bmatrix},$$

$$G(x) = \begin{bmatrix} b_2 \sin(x_1) \\ b_3 \sin(x_2) \end{bmatrix},$$

where a_1, b_2, b_3 are constant parameters we got from system identification.

The measurement vector is defined as follow:

$$
\begin{aligned}
&y = h(x) + v = [h_1, h_2, h_3, h_4]^T + v, \\
&h_1 = \dot{x}_1, h_2 = \dot{x}_2, h_3 = -g\sin(x_1), h_4 = -g\sin(x_2),
\end{aligned}
\tag{4.24}
$$

where h_1, $h_3 \in \mathbb{R}$ are angular velocities and h_2, $h_4 \in \mathbb{R}$ are gravitational acceleration projection on X axis of IMU sensor, all these singal have been transformaed to body coordinate system. Noise and drift are introduced in simulation to simulate a real environment. The acceleration measurement from IMU is a combination of gravitational acceleration and motion acceleration, in this case, only gravitational acceleration is considered because motion acceleration is negligible. The v is a four dimensional zero-mean Gaussian measurement noise with the measurement covariance matrix $S \in \mathbb{R}^{4\times4}$.

The chosen of SDC parametrization of this dynamic follow the method referred before in Section 4.1.2. The suitable SDC parametrization forms were chosen as follows:

$$
A(x,t) = \begin{bmatrix} 0 & 0 & 1 & 0 \\ 0 & 0 & 0 & 1 \\ A_{31} & A_{32} & A_{33} & A_{34} \\ A_{41} & A_{42} & A_{43} & A_{44} \end{bmatrix},
$$

$$
\begin{aligned}
A_{31} &= -w_{11}(b_2\mathrm{sinc}(x_1)), \\
A_{32} &= -w_{12}(b_3\mathrm{sinc}(x_2)), \\
A_{33} &= w_{12}a_1x_3\sin(x_1 - x_2), \\
A_{34} &= -w_{11}a_1x_4\sin(x_1 - x_2), \\
A_{41} &= -w_{21}(b_2\mathrm{sinc}(x_1)), \\
A_{42} &= -w_{22}(b_3\mathrm{sinc}(x_2)), \\
A_{43} &= w_{22}a_1x_3\sin(x_1 - x_2), \\
A_{44} &= -w_{21}a_1x_4\sin(x_1 - x_2),
\end{aligned}
$$

$$B\big(x(t)\big)U=\begin{bmatrix}0\\0\\M^{-1}(T_{pa}+T)\end{bmatrix},$$

$$C(x,t)=\begin{bmatrix}0 & 0 & 1 & 0\\ 0 & 0 & 0 & 1\\ -g\text{sinc}(x_1) & 0 & 0 & 0\\ 0 & -g\text{sinc}(x_2) & 0 & 0\end{bmatrix}. \tag{4.25}$$

Note: in order to meet the requirement of SDC form and original input have been rewrite as $U\in\mathbb{R}^7$.

The estimator construction is same as single joint model expect the change of dimension.

4.2.3 Simulation result and discussion

In order to fairly compare the performance of these two estimators, these two estimators were constructed in the same Simulink file, sharing the same IMU data. A small constant was introduced to the measurement of the gyroscope to simulate the IMU measurement drift. Radom noise was added to accelerometer measurement to simulate the measurement noise. The simulated IMU raw signal is shown in Figure 15 and Figure 16, it was very similar to the actual signal we measured in the experiment.

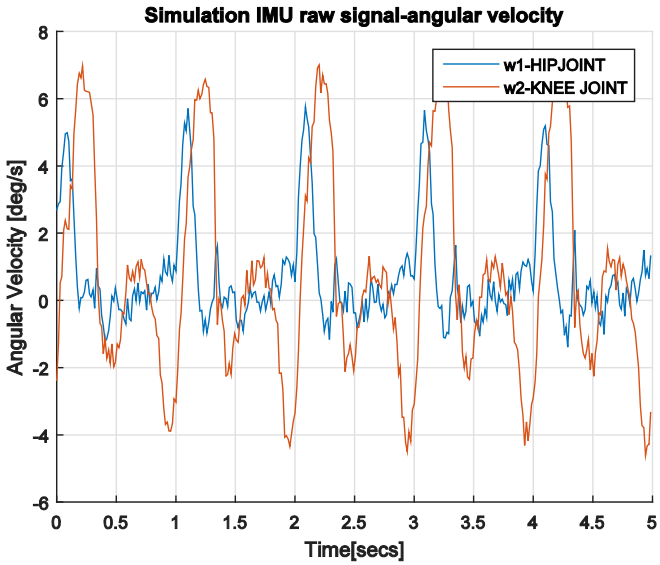

Figure 15. Simulation IMU signal-angular velocity

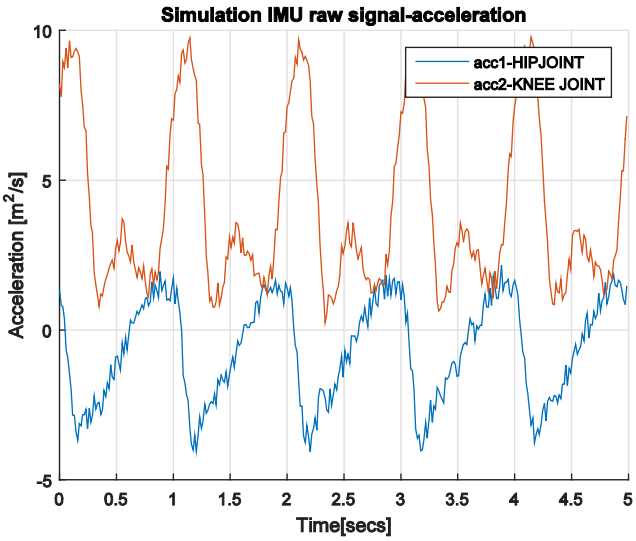

Figure 16. Simulation IMU signal-angular acceleration

Figure 17 shows the estimation results comparison between the SDRE estimator and EKF. The SDRE result almost matches the actual value while the EKF result tracks the real value with some error.

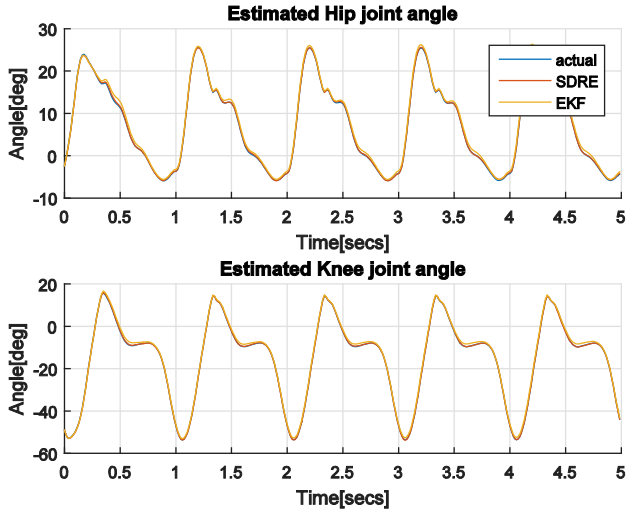

Figure 17. Simulation result comparison between SDRE estimator and EKF

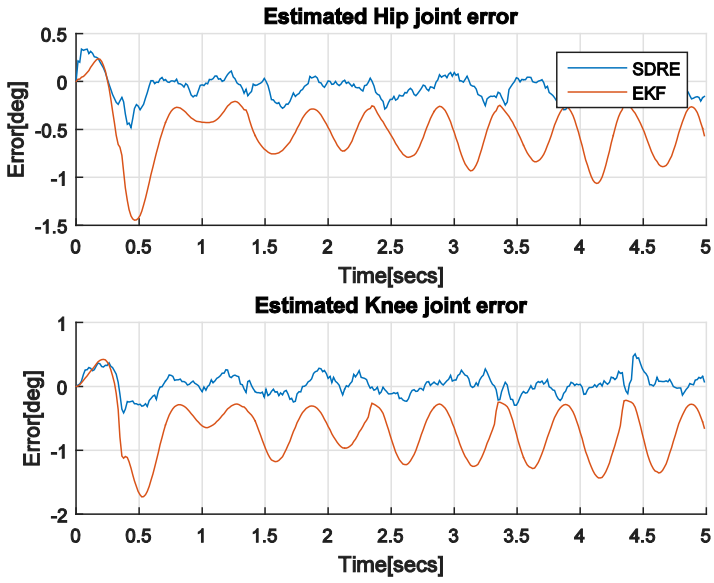

Figure 18. Error Comparison between SDRE estimator and EKF in Simulation

More details were provided in Figure 18, as we can see the error of SDRE estimator is very small with an RMSE about 0.2° and 0.23° for hip and knee joint. Compare to SDRE-estimator, the error of EKF is much larger.

Comparing to the estimation results of one joint model, the advantage of SDRE estimator become more apparent in the complex nonlinear system during the simulation study. It maybe because the SDC parameterization process preserves all details of nonlinear dynamics, but the application of Jacobian in EKF during linearization process approximates the original system. Another problem is that the errors of these two estimators in the simulation are much smaller than the errors in the experiment. This larger estimation error in the real experiment may result from inaccurate parameter identification or incomplete IMU frame transformation.

In order to figure out the influence of these two factors referred above, a set of simulation studies were performed as follows. In the first test, the dynamic model parameters was changed

to simulate the dynamic model we obtained by system identification in experiment which exist some error between the actual dynamic. The IMU drift and measurement noise were set as 0 to eliminate the influence of the measurement. As Figure 19 shows, both SDRE estimator and EKF appeared errors larger than before. The inaccurate dynamics caused by system identification may be one of the main cause of estimation error in experiment. It is noted that the changing of threshold value and initial angle of the dynamics were excluded in this simulation while we already know the changing of these two value may affect the overall estimation performance.

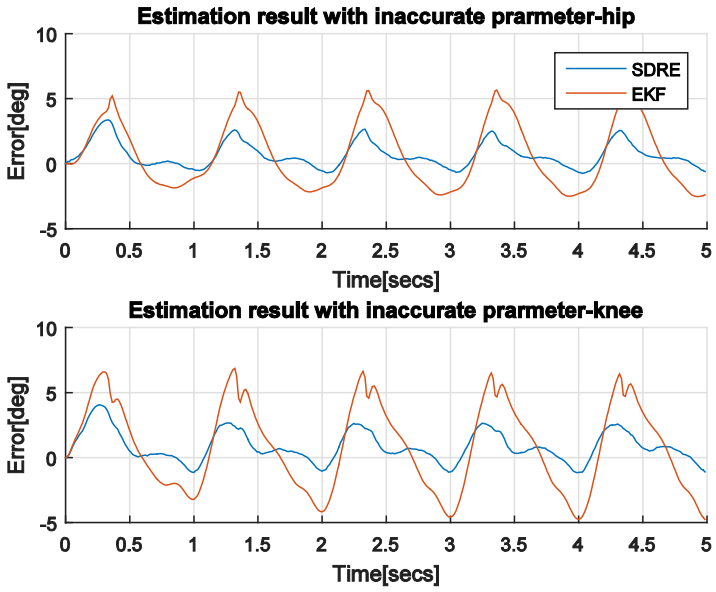

Figure 19. Estimation result with inaccurate dynamics

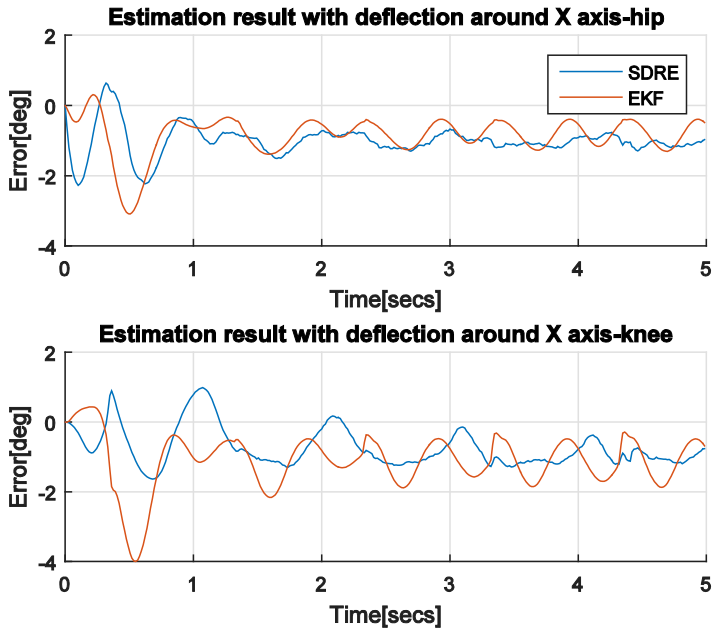

Figure 20. Estimation result with improper IMU alignment-1

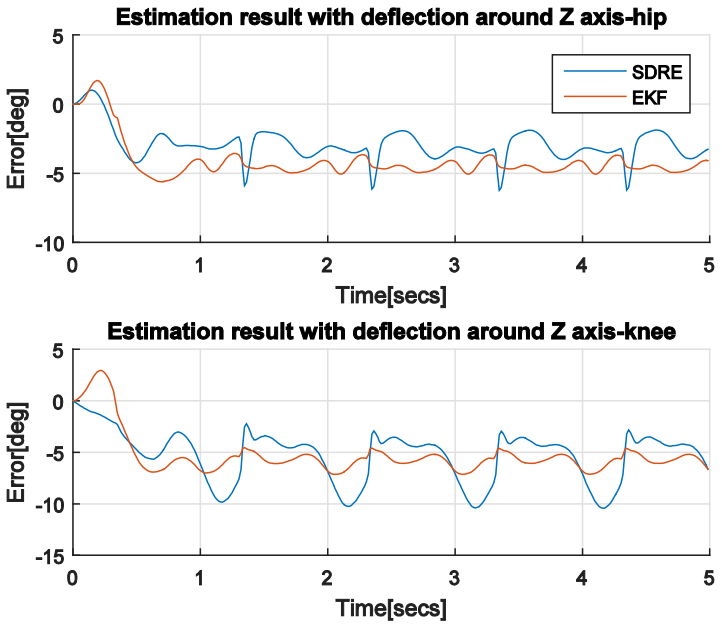

Figure 21. Estimation result with improper IMU alignment-2

Another set of simulation studies were performed to test the influence of incomplete IMU frame alignment. The setting of these simulation were set as follow:

S1: A constant was added to the acceleration signal to simulate inaccurate acceleration measurement caused by body frame rotation around X axis.

S2: The acceleration signal was multiplied by 0.8 to simulate the body frame created by alignment rotated around the Z axis with a small angle.

As shown in Figure 20 and Figure 21, both SDRE estimator and EKF were drift from the actual value, it seems inaccurate acceleration signal of IMU caused by incomplete IMU alignment have a strong effect on estimation performance. Especially in Figure 21, the SDRE estimator seems effected more by the inaccurate measurement as described in the S2.

More simulate studies were performed to explore the performance of these two estimator with different level IMU gyroscope drift in measurement. The gyroscope drift was simulated by adding a small constant (range from 0.1 to 1) to the simulation IMU gyroscope signal on each data point. An integration operation was performed to test the affections of these man-made drift on conventional angle calculation method. As shown in Figure 21, the simulation drift resulted in inaccurate angle estimation result. Especially the level 3, the estimation error almost reached 90°.

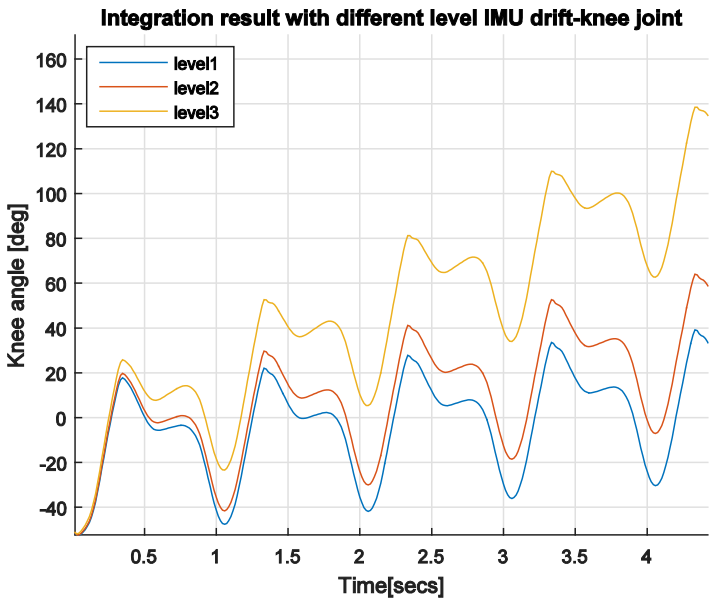

Figure 22. Integration result of gyroscope signal with different level drift

Then the EKF and SDRE-estimator were applied to estimate knee joint angles with these drift. Both of these two estimator were tuned to its best performance during these tests. As shown in Figure 23, the SDRE-estimator performed very well in knee joint angle estimation with different level IMU drift. The error of these three trials have very similar overall amplitude, which means the SDRE-estimator have a very strong ability to compensate the IMU measurement drift. The estimation result of EKF was shown in Figure 24, the EKF performed well when the IMU drift was small, and the amplitude of the estimation error was very close to the error of SDRE-estimator. But the estimation error became larger with IMU drift increased to level 3. It seems the ability to compensate IMU drift of EKF is not as good as SDRE-estimator.

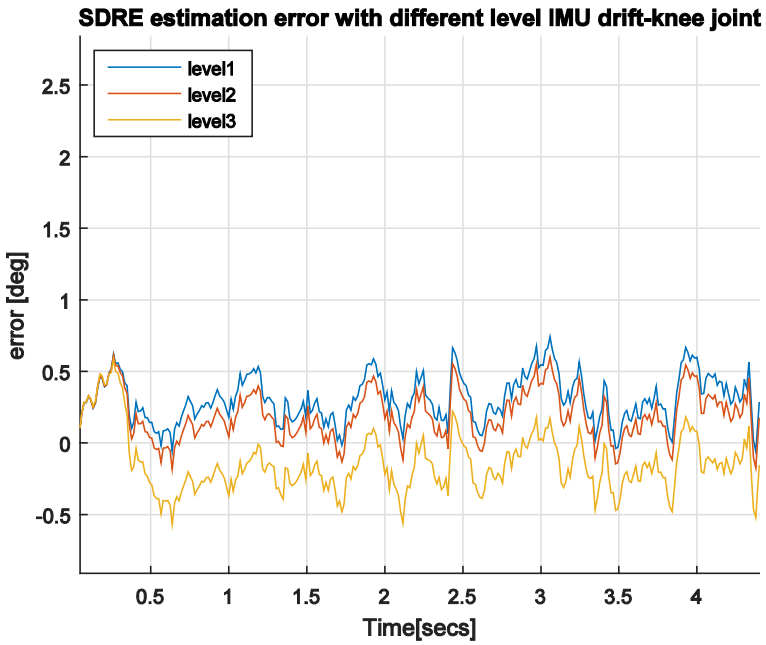

Figure 23. SDRE estimation error with different level drift

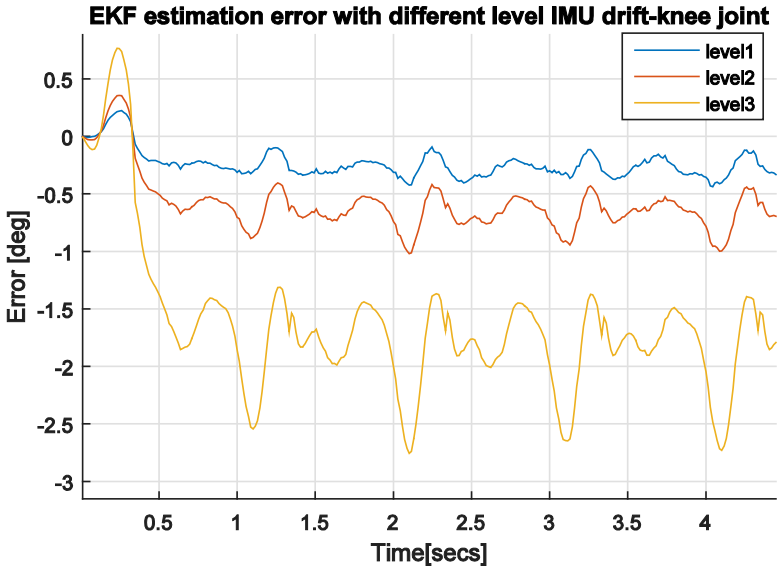

Figure 24. EKF estimation error with different level drift

Combining these simulation studies and results of single joint experiment, the larger error existed in the experiment might due to the inaccurate IMU measurement, especially the acceleration measurement and inaccurate system identification. The threshold value and initial

angle of dynamics also could influence the overall estimation result. More accurate system identification and IMU alignment algorithm are needed for improvement of SDRE estimator.

5.0 REAL-TIME ESTIMATION COUPLED WITH CONTROLLER

After design and implementation of the SDRE-estimator, this Chapter shows it online estimation. In the fixed hip model of the hybrid neuroprosthesis, the active torque of each joint can be produced by FES of joint flexors and extensors or electric motor, which introduced actuator redundancy problem. Our previous work [19] designed a lower dimensional controller inspired by muscle synergy principle specifically focused on solving the actuator redundancy problem, and it shows good performance on tracking. In this chapter, the proposed SDRE-estimator is coupled with the synergy based lower dimensional controller, the performance of this scheme was tested by a simulation study. The discussion about stability analysis for estimator-controller scheme is presented in Appendix B.

5.1 CONTROLLER DEVELOPMENT

The control objective is to track the desired trajectory, so the tracking error $e \in \mathbb{R}^2$ is defined as $e = q_d - \hat{q}$ define the auxiliary error signal $r \in \mathbb{R}^2$ is defined as

$$r = \dot{e} + \alpha e . \tag{5.1}$$

Choosing the update law as

$$u = W\hat{c} + kr , \tag{5.2}$$

where $\hat{c} \in \mathbb{R}^p$ is the estimate of c_d and $k \in \mathbb{R}^{6\times 2}$ is the feedback gain that is chosen only to effect the electric motors. The estimate of the principal components updates according to the following update law with the projection algorithm

$$\dot{\hat{c}} = proj\left(\dot{c}_d + \Gamma W^T b_d^T r\right), \tag{5.3}$$

while the $\Gamma \in \mathbb{R}^{p\times p}$ is a symmetric positive definite gain matrix. The stability analysis in [19] shows this synergy based adaptive closed loop control system is semi-global uniformly ultimately bounded (SGUUB)

5.2 SIMULATIONS

The developed controller-estimator scheme was tested in a simulation study on 2-DOF fixed hip model of a leg which can represent the gait cycle for when one leg fixed at the hip joint. There are six actuators in total including FES flexion, extension and an electric motor at each joint. The schematic of this model shown as Figure 14. In order to simulate the real performance of IMU sensor, we introduced constant noise into gyroscope measurement to simulate the IMU drift and introduced random noise into acceleration measurement. The Simulink block scheme is shown in Figure 28 in Appendix A.

5.3 RESULTS AND DISCUSSION

As expected, the SDRE estimator-adaptive controller scheme is sufficient to produce smooth limb motion. As shown in Figure 25, the estimation error is tiny regardless we introduced IMU

measurement drift and noise. As we can see at time 4.5 s, there appeared a larger disturbance but the estimator still converges back which shows its robustness. Figure 25 shows the tracking performance of estimator-controller pair. It is to be noted that although estimation error became slightly larger due to disturbance, the controller is still capable of tracking the desired trajectory with adaptive and feedback control.

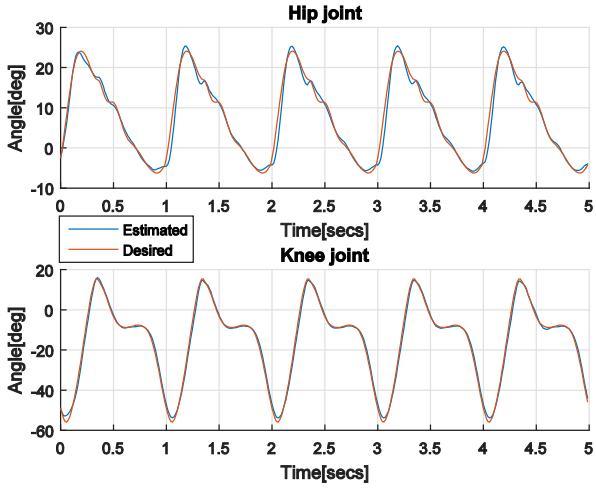

Figure 25. The joint angles resulting from simulating estimator-controller scheme. The top plot shows the desired and actual hip angle and the bottom plot shows the desired and actual knee angle, each for five steps.

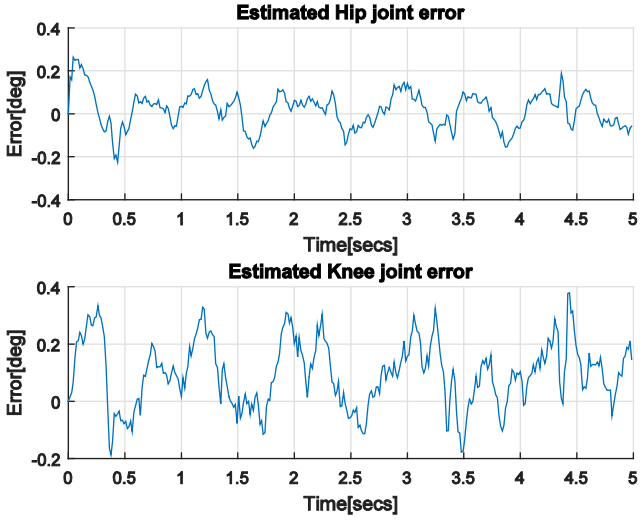

Figure 26. Estimation error of the SDRE-estimator

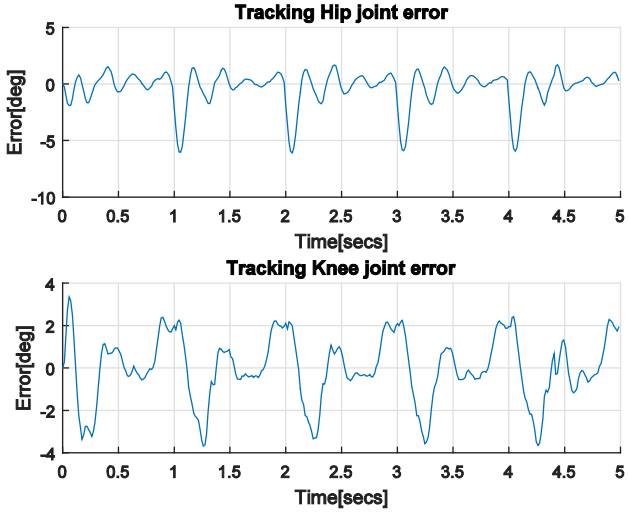

Figure 27. Joint motion tracking errors.

Figure 27 shows the tracking error of estimator-controller scheme.

6.0 CONCLUSION AND FUTURE WORK

This thesis presents the development of a wearable sensor-based estimator for functional electrical stimulation aided lower limb motion estimation. A new nonlinear estimator was designed to accurately estimate system state. This estimator was coupled with a controller and tested by a simulation study, a general framework for the stability analysis is given in Appendix B.

In the offline estimation study, estimators for one joint leg extension model and two joint fix hip model were designed and tested. The experimental validation indicated that for one joint model, the average RMSE of all trials was less than 1.77° between the SDRE-estimator estimated trajectory and the encoder recorded trajectory. The dynamic based EKF also performed well in this case with average RMSE about 2.04°. Compared to these dynamic model based estimators, the rotation matrix has larger average RMSE about 2.7°. The second part of offline estimation study was focused on applying these two dynamic based estimators to estimate motion base on fixed hip model by a simulation study. The simulation validation indicated that results of the SDRE-estimator and actual trajectories matched each other very well with near 0.2° RMSE on the hip joint and 0.23° RMSE on the knee joint while the RMSE of EKF was near 0.60° and 0.76° on hip and knee joint. This result proved the previous assumption that the SDRE-estimator performed better than EKF in complex nonlinear system with proper choose of SDC

form, and more accurate parameter identification and IMU alignment algorithm are needed for improvement of SDRE-estimator.

In Chapter 5, the newly designed estimator was coupled with a synergy inspired controller and tested by a simulation study. The simulation results indicate online estimation performance of SDRE-estimator was excellent with a very small error which is an ideal feedback signal to assure the tracking performance of the controller.

The dynamic model is the biggest limitation of this algorithm. As discussed in Chapter 4, the performance of SDRE-estimator highly relied on the accuracy of the dynamic model. By increasing the dynamic model's accuracy, the performance of this estimation algorithm can be greatly improved in the experiment. Also, the accuracy of acceleration measurement also play an important role in improving the performance of the estimator. Further work after this thesis should focus on improvement of parameter estimation accuracy and improve the matrix alignment procedure. Moreover, we also should continue testing the performance of this novel estimator-controller scheme in the experiment and further application on hybrid neuroprosthesis on walking.

APPENDIX A

ESTIMATOR-CONTROLLER SIMULATION BLOACK DIGRAM

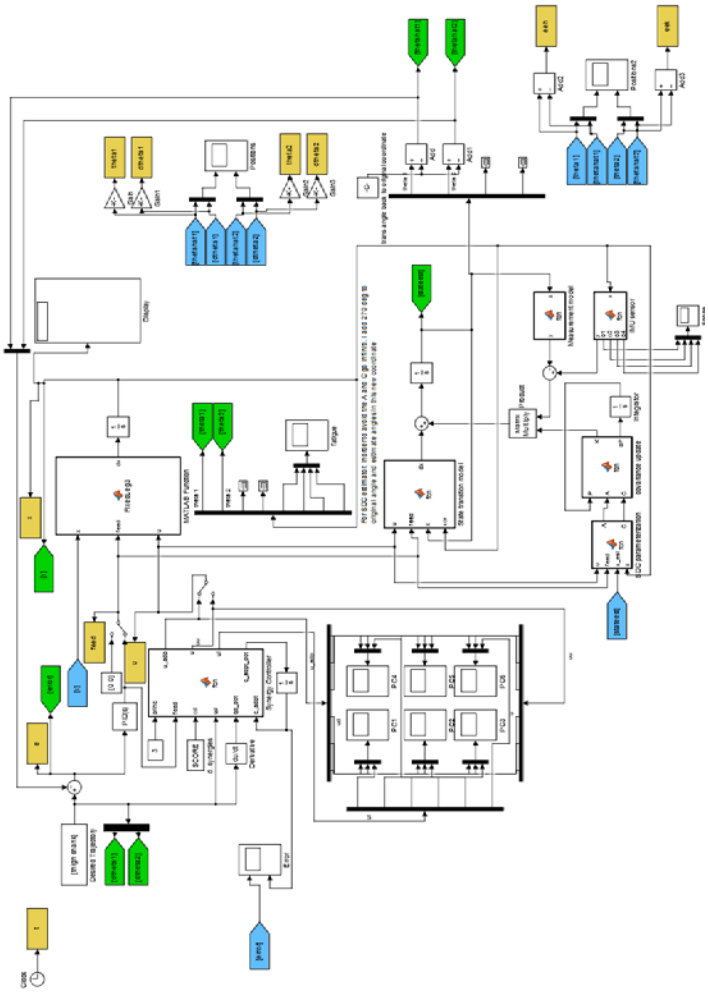

Figure 28. Simulink scheme of estimator-controller pair

APPENDIX B

DISCUSSION ABOUT STABILITY ANALYSIS of INTERCONNECTED SYSTEM

The overall dynamics of estimator-controller scheme can be shown as follow

$$\begin{aligned} \dot{x} &= f(t,x) + g(t,x)U(\hat{x}), \\ y &= h(t,x), \end{aligned} \tag{6.1}$$

$$\dot{\hat{x}} = A(\hat{x},t)\hat{x} + g(t,x)U(\hat{x}) + K(\hat{x},t)(y - C(\hat{x},t)\hat{x}), \tag{6.2}$$

the actual states x and estimated states $\hat{x}$ are shared by (6.1) and (6.2). As referred in 5.1, the controller is SGUUB, It is hard to directly prove the stability of this combination system. Some previous research has been done on this topic. Loria and Morals [34] applied nonlinear separation principle and cascade structure to prove the stability of the interconnected system. But in our case, the dual interconnected system cannot be directly rewritten into a form as cascade structure. In order to find a possible direction to prove the stability of estimator-controller scheme, we start to prove the stability of SDRE estimator.

Assumption 1. Follow the SDC parameterization method, the system (6.1) is transformable into the form

$$\dot{x} = A(x)x + W(x,U), \tag{6.3}$$

where the function $W(.)$ satisfies

$$\left\|W(x,U)-W(\hat{x},U)\right\|=\tilde{W}\le l_w\left\|e_f\right\|, \tag{6.4}$$

where $e_f=\hat{x}-x\forall x,\hat{x}\in\mathbb{R}^4\forall t\ge 0$.

Remark. The **Assumption 1** contain follow second layer assumptions:

$$\begin{aligned}&\left\|g(t,x)U-g(t,\hat{x})U\right\|=\tilde{W}\le l_w\left\|e_f\right\|,\\&\left\|g(t,x)-g(t,\hat{x})\right\|\le l_g\left\|e_f\right\|,\\&\left\|U\right\|\le l_u, l_u*l_g\left\|e_f\right\|\le l_w\left\|e_f\right\|,\end{aligned}$$

where l_g,l_w,l_u are positive constants. This assumption is based on [35] and [36], the l_u can be determined by considering the actuators saturation limit. Other researchers such as [37, 38], where SDRE estimator stability analysis are usually based on a dynamic system without system input, therefore the previous assumption can be avoided.

The SDRE estimator also can be written as

$$\dot{\hat{x}}=A(\hat{x},t)\hat{x}+W(\hat{x},U)+K(\hat{x},t)(y-C(\hat{x},t)\hat{x}). \tag{6.5}$$

Then the error dynamics of proposed SDRE estimator can be expressed as follow

$$\dot{e}_f=[A(\hat{x})-K(\hat{x})C(\hat{x})]e_f+\tilde{A}-K(\hat{x})\tilde{C}+\tilde{W}, \tag{6.6}$$

where

$$\begin{aligned}\tilde{A}&\triangleq(A(x)-A(\hat{x}))x,\\\tilde{C}&\triangleq(C(x)-C(\hat{x}))x.\end{aligned} \tag{6.7}$$

There exist some assumptions for the SDRE estimator as follow

Assumption 2. Following [39], the positive definite solution $P(\hat{x},t)$ of the differential Riccati (4.16) satisfies the bound

$$\underline{p}I\le P(\hat{x},t)\le\overline{p}I,\forall t\ge 0 \tag{6.8}$$

Assumption 3. As [38], the SDC parameterization $C_j(x)$ is such that

$$\left\|C(x,t)\right\| \le \overline{c} \tag{6.9}$$

where constant $\overline{c} \in \mathbb{R}^+$.

Assumption 4. The SDC parameterization $A(x)$ and $C(x)$ are chosen such that $L_a, L_c \in \mathbb{R}^+$ for all $x, \hat{x}$,

$$\begin{aligned} \left\|A(x)-A(\hat{x})\right\| &\le L_a \left\|x-\hat{x}\right\| \\ \left\|C(x)-C(\hat{x})\right\| &\le L_c \left\|x-\hat{x}\right\| \end{aligned} \tag{6.10}$$

Assumption 5. There exist $\sigma \in \mathbb{R}^+$ for all $t \ge 0$, $\left|x\right| \le \sigma$.

In order to analysis the stability of proposed estimator, the Lyapunov function $V(e) \in \mathbb{R}$ is defined as:

$$V = e_f^T P^{-1} e_f \,. \tag{6.11}$$

There exist lower bound and upper bound as

$$\frac{1}{\overline{p}}\left\|e_f\right\|^2 \le V_2 \le \frac{1}{\underline{p}}\left\|e_f\right\|^2. \tag{6.12}$$

Taking the time derivative of $V(x,\hat{x},t)$, then we got

$$\dot{V} = \dot{e}_f^T\, P^{-1} e_f + e_f^T \dot{P}^{-1} e_f + e_f^T P^{-1}\, \dot{e}_f \,, \tag{6.13}$$

according to **Assumptions 1-5** and $\left\|S^{-1}\right\| \le \frac{1}{\underline{s}}$ there exist follow inequality

$$\begin{aligned} e_f^T P^{-1}(\tilde{A}+\tilde{B}-K(\hat{x})\tilde{C}) &\le \left\|e_f^T P^{-1}(\tilde{A}+\tilde{B}-K(\hat{x})\tilde{C})\right\| \\ &\le \left\|e_f^T P^{-1}\tilde{A}\right\| + \left\|e_f^T P^{-1}\tilde{W}\right\| + \left\|e_f^T P^{-1}K(\hat{x})\tilde{C}\right\| \\ &\le \kappa\left\|e_f\right\|^2, \end{aligned} \tag{6.14}$$

where the constant $\kappa = \frac{L_a\sigma + L_w}{\underline{p}} + \frac{\overline{c}L_c\sigma}{\underline{s}}$.

Substituting (6.6) into $\dot{V}$, then following obtained:

$$\begin{aligned} \dot{V} = \quad & e_f^T \dot{P}^{-1} e_f + e_f^T P^{-1}(A(\hat{x}) - K(\hat{x})C(\hat{x}))e_f \\ & + e_f{}^T (A(\hat{x}) - K(\hat{x})C(\hat{x}))^T P^{-1} e_f + 2e_f^T P^{-1}(\tilde{A} + \tilde{B} - K(\hat{x})\tilde{C}), \end{aligned} \tag{6.15}$$

combining with (6.14) and (4.15), it can be further bounded as

$$\begin{aligned} \dot{V} \le \quad & e_f^T \left(\dot{P}^{-1} + P^{-1}A(\hat{x}) + A^T(\hat{x})P^{-1} \right) e_f \\ & e_f^T \left(-2C^T(\hat{x})R^{-1}C(\hat{x}) \right) e_f + 2\kappa \left\| e_f \right\|^2. \end{aligned} \tag{6.16}$$

Considering

$$\dot{P}^{-1} = -P^{-1}\dot{P}P^{-1},$$

combine with the Riccati differential equation (4.16) leads to

$$\begin{aligned} \dot{V} \le \quad & -e_f^T \left(P^{-1}QP^{-1} + C^T R^{-1} C \right) e_f \\ & -2\alpha e_f^T P^{-1} e_f + 2\kappa \left\| e_f \right\|^2. \end{aligned} \tag{6.17}$$

Denoting the smallest eigenvalue of the positive-definite matrix Q by $\underline{q}$, we have $0 \le \underline{q}I \le Q$.

Together with **Assumption 2** for P we obtain

$$\dot{V} \le -2aV + (-\frac{q}{\overline{p}^2} + 2\kappa) \left\| e_f \right\|^2, \tag{6.18}$$

moreover from above that

$$\dot{V} \le (-2a - \frac{qp}{\overline{p}^2} + 2\kappa \underline{p})V. \tag{6.19}$$

If the gain a is taken large enough, i.e., $a > -\frac{\overline{qp}}{2\overline{p}^2} + \kappa \underline{p}$ the globally exponential uniformly stability of the state estimation can be achieved since the derivative of $V(e)$ will be negative definite.

By applying $U = k(t, \hat{x})$, the original system (6.1) can be expressed as follow:

$$\dot{x} = f(t,x) + g(t,x)k(t,x) + g(t,x)\left[k(t,\hat{x}) - k(t,x)\right]. \tag{6.20}$$

Assumption 6. For the function $\mathrm{g}(t,x)$ and $k(t,x)$ there exist nondecreasing function $\theta(.)$ that

$$\left\|\mathrm{g}(t,x)\right\| \le \theta_1(|x|)\forall x \in \mathbb{R}^4, \tag{6.21}$$

$$\left\|k(t,\hat{x}) - k(t,x)\right\| \le \theta_2(|\hat{x} - x|)\forall x, \hat{x} \in \mathbb{R}^4. \tag{6.22}$$

The overall interconnected system can be expressed as follow:

$$\dot{x} = f(t,x) + g(t,x)k(t,x) + g(t,x)\left[k(t,\hat{x}) - k(t,x)\right], \tag{6.23}$$

$$\dot{e}_f = [A(\hat{x}) - K(\hat{x})C(\hat{x})]e_f + \tilde{A} - K(\hat{x})\tilde{C} + \tilde{W}. \tag{6.24}$$

Inspired by [34], a key observation to this point is that the estimator error dynamics is globally exponentially stable, that means even the error dynamics (6.24) is related to the actual state x, the estimation error e_f trend to zero exponentially for any trajectory x .Therefore, the stability of error dynamic of the estimator can be assumed as not related to x.

By defining $\zeta = col[x, e_f]$, the overall system can be written on the cascade structure as follow

$$\begin{aligned} \dot{\zeta}_1 &= F_1(t,\zeta_1) + G(t,\zeta)\alpha(t,\zeta), \\ \dot{\zeta}_2 &= F_0(t,\zeta_2), \end{aligned} \tag{6.25}$$

where $G(t,\zeta) = g(t,\zeta)$, $\alpha(t,\zeta) = \left[k(t,\zeta) - k(t,\zeta_1)\right]$.

According to Theorem 1 in [40], the cascaded system (6.25) referred above will keep the stability characteristic of the original closed loop system which is semi-global ultimate uniformly stable (SGUUB).

A general framework for stability analyze of estimator-controller scheme is given. A strong assumption (**Assumption 1**) was to support the proof. The future work will focus on removing this strong assumption.

BIBLIOGRAPHY

[1] National Spinal Cord InjuryStatistical, C., *Spinal Cord Injury Facts and Figures at a Glance.* The journal of spinal cord medicine, 2014. **37**(3): p. 355-356.

[2] Kobetic, R., R.J. Triolo, and E.B. Marsolais, *Muscle selection and walking performance of multichannel FES systems for ambulation in paraplegia.* IEEE Transactions on Rehabilitation Engineering, 1997. **5**(1): p. 23-29.

[3] del-Ama, A.J., A. Gil-Agudo, J.L. Pons, and J.C. Moreno, *Hybrid FES-robot cooperative control of ambulatory gait rehabilitation exoskeleton.* Journal of neuroengineering and rehabilitation, 2014. **11**(1): p. 27-27.

[4] Thrasher, T.A., V. Zivanovic, W. McIlroy, and M.R. Popovic, *Rehabilitation of Reaching and Grasping Function in Severe Hemiplegic Patients Using Functional Electrical Stimulation Therapy.* Neurorehabilitation and Neural Repair, 2008. **22**(6): p. 706-714.

[5] Rushton, D.N., *Functional Electrical Stimulation and rehabilitation—an hypothesis.* Medical Engineering and Physics, 2003. **25**(1): p. 75-78.

[6] Kobetic, R., C.S. To, J.R. Schnellenberger, M.L. Audu, T.C. Bulea, R. Gaudio, G. Pinault, S. Tashman, and R.J. Triolo, *Development of hybrid orthosis for standing, walking, and stair climbing after spinal cord injury.* Journal of rehabilitation research and development, 2009. **46**(3): p. 447.

[7] Farris, R.J., H.A. Quintero, and M. Goldfarb, *Preliminary Evaluation of a Powered Lower Limb Orthosis to Aid Walking in Paraplegic Individuals.* IEEE Transactions on Neural Systems and Rehabilitation Engineering, 2011. **19**(6): p. 652-659.

[8] Goldfarb, M., K. Korkowski, B. Harrold, and W. Durfee, *Preliminary evaluation of a controlled-brake orthosis for FES-aided gait.* IEEE Transactions on Neural Systems and Rehabilitation Engineering, 2003. **11**(3): p. 241-248.

[9] Mayagoitia, R.E., A.V. Nene, and P.H. Veltink, *Accelerometer and rate gyroscope measurement of kinematics: an inexpensive alternative to optical motion analysis systems.* Journal of Biomechanics, 2002. **35**(4): p. 537-542.

[10] Pappas, I.P.I., M.R. Popovic, T. Keller, V. Dietz, and M. Morari, *A reliable gait phase detection system.* IEEE Transactions on Neural Systems and Rehabilitation Engineering, 2001. **9**(2): p. 113-125.

[11] Riel, W.J.B.M., P.H. Veltink, and C.C. Monaghan, *Control of triceps surae stimulation based on shank orientation using a uniaxial gyroscope during gait.* Medical and biological engineering and computing, 2009. **47**(11): p. 1181-1188.

[12] Hermens, H.J., P.H. Veltink, and D. Kotiadis, *Inertial Gait Phase Detection for control of a drop foot stimulator: Inertial sensing for gait phase detection.* Medical Engineering & Physics, 2010. **32**(4): p. 287-297.

[13] Williamson, R. and B.J. Andrews, *Detecting absolute human knee angle and angular velocity using accelerometers and rate gyroscopes.* Medical & Biological Engineering & Computing, 2001. **39**(3): p. 294-302.

[14] Stein, R.B., D.G. Everaert, A.K. Thompson, S.L. Chong, M. Whittaker, J. Robertson, and G. Kuether, *Long-Term Therapeutic and Orthotic Effects of a Foot Drop Stimulator on Walking Performance in Progressive and Nonprogressive Neurological Disorders.* Neurorehabilitation and Neural Repair, 2010. **24**(2): p. 152-167.

[15] Veltink, P.H. and H.J. Luinge, *Measuring orientation of human body segments using miniature gyroscopes and accelerometers.* Medical and biological engineering and computing, 2005. **43**(2): p. 273-282.

[16] Bennett, T., R. Jafari, and N. Gans. *An extended Kalman filter to estimate human gait parameters and walking distance*. IEEE.

[17] Joukov, V., M. Karg, and D. Kulic. *Online tracking of the lower body joint angles using IMUs for gait rehabilitation*. United States: IEEE.

[18] Fourati, H., N. Manamanni, L. Afilal, and Y. Handrich. *Position estimation approach by Complementary Filter-aided IMU for indoor environment*. EUCA.

[19] Alibeji, N.A., N.A. Kirsch, and N. Sharma, *A Muscle Synergy-Inspired Adaptive Control Scheme for a Hybrid Walking Neuroprosthesis.* Frontiers in bioengineering and biotechnology 2015. **3**: p. 203.

[20] Glaser, R.M., *Functional Neuromuscular Stimulation.* International Journal of Sports Medicine, 2008. **15**(3): p. 142-148.

[21] Liberson WT, H.H., Scot D, and D. M, *Functional electrotherapy: stimulation of the peroneal nerve synchronized with the swing phase of the gait of hemiplegic patients.* Arch. Phys. Med. Rehabil., 1961. **42**: p. 101-5.

[22] P. Hunter Peckham, J.S.K., *FUNCTIONAL ELECTRICAL STIMULATION FOR NEUROMUSCULAR APPLICATIONS.* Annual review of biomedical engineering, 2005. **7**: p. 327-60.

[23] Kralj A, B.T., Turk R., *Electrical stimulation providing functional use of paraplegic patient muscles.* . Med. Prog. Technol. **7**: p. 3-9.

[24] Graupe D, K.K., *Functional neuromuscular stimulator for shortdistance ambulation by certain thoraciclevel spinal-cord-injured paraplegics.* Surg. Neurol., 1998. **50**: p. 202-7.

[25] Marsolais EB, K.R., *Functional electrical stimulation for walking in paraplegia.* . 1987. **69**: p. 728-33.

[26] Mazzà, C., M. Donati, J. McCamley, P. Picerno, and A. Cappozzo, *An optimized Kalman filter for the estimate of trunk orientation from inertial sensors data during treadmill walking.* Gait & posture, 2012. **35**(1): p. 138-142.

[27] Masdar, A., B.S.K.K. Ibrahim, D. Hanafi, M.M.A. Jamil, and K.A.A. Rahman. *Knee joint angle measurement system using gyroscope and flex-sensors for rehabilitation*. IEEE.

[28] Lovse, L., J. Bobet, F.D. Roy, R. Rolf, V.K. Mushahwar, and R.B. Stein, *External sensors for detecting the activation and deactivation times of the major muscles used in walking.* IEEE transactions on neural systems and rehabilitation engineering 2012. **20**(4): p. 488-498.

[29] https://en.wikipedia.org/wiki/Inertial_measurement_unit, *Description of inertial measurement unit.*

[30] http://www.starlino.com/imu_guide.html, *A Guide To using IMU (Accelerometer and Gyroscope Devices) in Embedded Applications.*

[31] http://www.patentstorm.us/patents/5067084/description.html, *Description of IMU aiding from Roll isolated Gyro.*

[32] https://www.yostlabs.com/yost-labs-3-space-sensors-low-latency-inertial-motion-capture-suits-and-sensors, *Description of 3 Space sensor.*

[33] N. Kirsch, N.A., and N. Sharma, *Nonlinear Model Predictive Control of Functional Electrical Stimulation.* Control Engineering Practice.

[34] Loria, A., T.I. Fossen, and E. Panteley, *A separation principle for dynamic positioning of ships: Theoretical and experimental results.* IEEE Transactions on Control Systems Technology, 2000. **8**(2): p. 332-343.

[35] Ablay, G., *Robust estimator-based optimal control designs for U-tube steam generators.* Transactions of the Institute of Measurement and Control, 2015. **37**(5): p. 636-644.

[36] Beikzadeh, H. and H.D. Taghirad, *Exponential nonlinear observer based on the differential state-dependent Riccati equation.* International Journal of Automation and Computing, 2012. **9**(4): p. 358-368.

[37] Jaganath, C., A. Ridley, and D.S. Bernstein, *A SDRE-based asymptotic observer for nonlinear discrete-time systems.* Proceedings of the 2005, American Control Conference, 2005., 2005: p. 3630-3635.

[38] Dani, A.P., S.-J. Chung, and S. Hutchinson, *Observer Design for Stochastic Nonlinear Systems via Contraction-Based Incremental Stability.* IEEE Transactions on Automatic Control, 2015. **60**(3): p. 700-714.

[39] Reif, K., F. Sonnemann, and R. Unbehauen, *An EKF-Based Nonlinear Observer with a Prescribed Degree of Stability.* Automatica, 1998. **34**(9): p. 1119-1123.

[40] Panteley, E. and A. Loria, *On global uniform asymptotic stability of nonlinear time-varying systems in cascade.* Systems & Control Letters, 1998. **33**(2): p. 131-138.